

# **A roadmap to Estimating—estimating agricultural ammonia volatilization over Europe using satellite observations and simulation data using IASI and GEOS-Chem**

Rimal Abeed<sup>1</sup>, Camille Viatte<sup>1</sup>, William C. Porter<sup>2</sup>, Nikolaos Evangeliou<sup>3</sup>, Cathy Clerbaux<sup>1,4</sup>, Lieven Clarisse<sup>4</sup>, Martin Van Damme<sup>4,5</sup>, Pierre-François Coheur<sup>4</sup>, and Sarah Safieddine<sup>1</sup>

<sup>1</sup>LATMOS/IPSL, Sorbonne Université, UVSQ, CNRS, Paris, France

<sup>2</sup>Department of Environmental Sciences, University of California, Riverside, CA 92521, USA

<sup>3</sup>Norwegian Institute for Air Research (NILU), Department of Atmospheric and Climate Research (ATMOS), Kjeller, Norway

<sup>4</sup>Université libre de Bruxelles (ULB), Spectroscopy, Quantum Chemistry and Atmospheric Remote Sensing (SQUARES), Brussels, Belgium

<sup>5</sup>Belgian Institute for Space Aeronomy (BIRA-IASB), Brussels 1180, Belgium

Correspondence to: Rimal Abeed [rimal.abeed@latmos.ipsl.fr](mailto:rimal.abeed@latmos.ipsl.fr)

## **Abstract**

Ammonia (NH<sub>3</sub>) is one of the most important gases emitted from agricultural practices. It affects air quality and the overall climate, and in turn influenced by long term climate trends as well as by short term fluctuations in local and regional meteorology. Previous studies have established the capability of the Infrared Atmospheric Sounding Interferometer (IASI) series of instruments aboard the Metop satellites to measure ammonia from space since 2007. In this study, we explore the interactions between atmospheric ammonia, land and meteorological variability, and long-term climate trends in Europe. We investigate the emission potential ( $\Gamma_{soil}$ ) of ammonia from the soil, which describes the soil – atmosphere ammonia exchange.  $\Gamma_{soil}$  is generally calculated in-field or in laboratory experiments; here, and for the first time, we investigate a method which assesses it remotely using satellite data, reanalysis data products, and model simulations.

We focus on ammonia emission potential during March 2011, which marks the start of growing season in Europe. Our results show that  $\Gamma_{soil}$  ranges from  $2 \times 10^3$  to  $9.5 \times 10^4$  (dimensionless) in a fertilized cropland, such as in the North European Plain, and is of the order of  $10 - 10^2$  in a non-fertilized soil (e.g. forest and grassland). These results agree with in-field measurements from the literature, suggesting that our method can be used in other seasons and regions in the world. However, some improvements are needed in the determination of mass transfer coefficient  $k$  (m s<sup>-1</sup>), which is a crucial parameter to derive  $\Gamma_{soil}$ .

Using a climate model, we estimate the expected increase in ammonia columns by the end of the century based on the increase in skin temperature (T<sub>skin</sub>), under two different climate scenarios. Ammonia columns are projected to increase by up to 50 %, particularly in Eastern Europe, under the SSP2-4.5 scenario, and might even double (increase of 100 %) under the SSP5-8.5 scenario. The increase in skin temperature is responsible for a formation of new hotspots of ammonia in Belarus, Ukraine, Hungary, Moldova, parts of Romania, and Switzerland.

49  
50  
51

## 52 1. Introduction

53 Ammonia ( $\text{NH}_3$ ) emissions have been increasing in a continuous manner from 1970 to 2017 (McDuffie et al., 2020). During  
54 the period 2008 – 2018 alone, the increase in ammonia columns in Western and Southern Europe ~~accounted~~ amounted to 20.8  
55 %  $\text{yr}^{-1}$  ( $\pm 4.3$  %), and to 12.8 ( $\pm 1.3$  %) globally (Van Damme et al., 2021). Although ammonia alone is stable against heat and  
56 light, it is considered a very reactive base, ~~whereas~~ and it constitutes the largest portion of the reactive nitrogen ( $\text{N}_r$ ) on Earth.  
57 The vast majority of atmospheric ammonia not deposited is transformed into fine particulate matter ( $\text{PM}_{2.5}$ ) composed of  
58 ammonium ( $\text{NH}_4^+$ ), through acid – base chemical reactions with available acids in the environment, namely sulfuric acid  
59 ( $\text{H}_2\text{SO}_4$ ), hydrochloric acid (HCl), and nitric acid ( $\text{HNO}_3$ ) (Yu et al., 2018), while only 10 % of the total ammonia gas ~~are~~ is  
60 believed to be oxidized by hydroxyl radicals ( $\text{OH}^\cdot$ ) (Roelle and Aneja, 2005).  $\text{PM}_{2.5}$  has degrading effects on human health,  
61 especially respiratory diseases (Bauer et al., 2016). ~~In addition to agriculture, ammonia can be emitted from industrial processes,~~  
62 ~~biomass burning (Van Damme et al., 2018), and natural activities such as from seal colonies (Theobald et al., 2006).~~

63  
64 Soils are known to be a source of atmospheric ammonia, especially in areas of intensive agricultural practices (Schlesinger and  
65 Hartley, 1992), and this is due to enriching the soil with the reactive nitrogen present in fertilizers. The increase in the  
66 application of synthetic fertilizers, and intensification of agricultural practices is believed to be the dominant factor of the global  
67 increase in ammonia emissions over the past century (Behera et al., 2013; McDuffie et al., 2020). ~~In addition to agriculture,~~  
68 ~~ammonia can be emitted from industrial processes, biomass burning (Van Damme et al., 2018), and natural activities~~ sources  
69 ~~such as from seal colonies (Theobald et al., 2006).~~

70  
71 Following the application of fertilizers, ammonium and ammonia are released in the soil. Prior to its volatilization, ammonia  
72 in the soil exists either in the gas phase ( $\text{NH}_3(\text{g})$ ) or in the aqueous/liquid phase ( $\text{NH}_3(\text{aq})$ ), the equilibrium between both states  
73 of ammonia is governed by Henry's law (Wentworth et al., 2014), as shown in ~~the Appendix-A~~. The dissociation of ammonia  
74 in soil water is ~~affected~~ a function of soil acidity (pH) and temperature (Roelle and Aneja, 2005) (Eq. (A-1)(A-1) and (A-  
75 2)(A-2) in Appendix A); ~~it is, and controlled~~ explained by the dissociation constant  $K_{\text{NH}_4^+}$ . Once released to the atmosphere,  
76 ammonia near the surface exists in the gas phase, hence Henry's law ~~can be used to~~ describes the equilibrium between  
77 ammonia in the soil (liquid phase), and near the surface (gas phase). This bi-directional exchange between the soil and the  
78 atmosphere will continue until the equilibrium is reached, and this occurs when ammonia concentration is equal to the  
79 compensation point  $\chi_{\text{NH}_3}$  (the concentration of ammonia at equilibrium). The flux of ammonia from the soil to the atmosphere  
80 (emission) occurs when the concentration of atmospheric ammonia is less than the compensation point  $\chi_{\text{NH}_3}$ , while ammonia  
81 deposition occurs when the concentration of ammonia is equal to or greater than  $\chi_{\text{NH}_3}$  (Flechard et al., 2011; Wichink Kruit,  
82 2010). It is then crucial to quantify the compensation point in order to understand this bi-directional exchange. The main  
83 variables needed to calculate  $\chi_{\text{NH}_3}$  are soil temperature ( $T_{\text{skin}}$ ) and  $\Gamma_{\text{soil}}$ , which is a dimensionless ratio between ammonium  
84 and pH ( $\text{NH}_4^+(\text{aq})$  and  $\text{H}^+(\text{aq})$  concentrations, respectively, in the soil). All the equations are described in Appendix A (Eq.  
85 (A-1)(A-1) to (A-15)(A-15)).

86  
87 The soil emission potential ( $\Gamma_{\text{soil}}$ ) has been thoroughly investigated in field and controlled laboratory environments (e.g. David  
88 et al., 2009; Flechard et al., 2013; Massad et al., 2010; Mattsson et al., 2008; Nemitz et al., 2000; Wentworth et al., 2014,  
89 among others).  $\Gamma_{\text{soil}}$  is dimensionless and it can range from 20 (non-fertilized soil in a forest) to the order of  $10^6$  (mixture of  
90 slurry in a cropland). It is found to peak right after fertilizers application, due to the increase in ammonium content in the soil  
91 (a product of urea hydrolysis), ~~reaching~~ and to return to pre-fertilization levels 10 days ~~following~~ after the application (Flechard  
92 et al., 2010; Massad et al., 2010). Little information exists on regional or global scales to assess the large-scale spatial variability  
93 of ammonia emission potentials.

94  
95 In order to meet the needs ~~offer~~ a growing population, agricultural practices have intensified during the ~~period~~ 2003 – 2019  
96 ~~period~~ (more fertilizer use per surface area), resulting in ~~an~~ increased in the net primary production (NPP) per capita (Potapov  
97 et al., 2022); ~~subsequently increasing~~ and volatilized ammonia (due to increase in ~~both~~ nitrogen soil content, and cultivated  
98 lands). In Europe alone, the area of croplands increased by 9 % from 2003 to 2019, and most of the expansion took place on  
99 lands that were abandoned for more than 4 years (Potapov et al., 2022). ~~Between the year 2008 and 2018, the increase in~~  
100 ~~atmospheric ammonia columns~~ accounted to 20.8 % ( $\pm 4.3$  %) in Western and Southern Europe (Van Damme et al., 2021).  
101 ~~Around 90 % of the mineral fertilizers used in Europe are nitrogen-based, with urea and nitrate fertilizers dominating the market~~

in the 27 EU countries, since they make up 22 % and 45 % of the total market (Fertilizers Europe, 2016). With the increase in croplands area and agricultural activities, climate change will have a significant effect on agricultural practices, with warmer climates enhancing the volatilization of ammonia from soils, especially in intensely fertilized lands (Shen et al., 2020).

This study aims at exploring ammonia emission potential and volatilization in Europe, using infrared satellite data of ammonia columns, reanalysis temperature data, and chemical transport model simulations to provide information on chemical sources and sinks. We specifically study the relationship between satellite-derived ammonia concentration at the start of the growing season, soil emission potentials and their spatial variability over Europe during March of 2011. Section 2 provides the methods/datasets used. The results are described in Sect. 3, including simulation from GEOS-Chem in Sect. 3.1 and regional Regional emission potentials are shown and discussed in Sect. 3.23-24. Using a climate model, future projections of ammonia columns are investigated under different climate scenarios in Sect. 3.33-35. Discussion and Conclusions are listed in Sect. 4.

## 2. Methodology

### 2.1. Calculation of the emission potential

In this study, we use IASI satellite data to calculate the ammonia emission potential  $\Gamma_{soil}$  instead of field soil measurements. In field studies,  $\Gamma_{soil}$  is calculated by measuring the concentration of ammonium ( $\text{NH}_4^+$ ) and  $\text{H}^+$  ( $10^{\text{pH}}$ ) in the soil; the ratio between both of these concentrations is  $\Gamma_{soil}$ . In this study here, we use infrared satellite ammonia observations which offer to have a regional coverage over Europe. With these, however, we cannot monitor soil content of ammonium nor its pH. This renders the remote  $\Gamma_{soil}$  calculation challenging, and less straight forward. The full derivation of the equation used to calculate the emission potential is explained in Appendix A, and was briefly described in the introduction. In short, upon its dissolution in the soil water, ammonia follows Henry's law. In steady state conditions between the soil and the near surface, the amount of the ammonia emitted and lost is considered equal. Based on this assumption, the soil emission potential (dimensionless) is calculated as follows Eq. (2-1) or Eq. (A-15) in Appendix A:

$$\Gamma_{soil} = \frac{[\text{NH}_3]^{col} \cdot T_{soil}}{\exp\left(\frac{-b}{T_{soil}}\right)} \frac{M_{\text{NH}_3}}{a \cdot N_a \cdot c'} \frac{1}{k\tau} \quad (2-1)$$

where  $[\text{NH}_3]^{col}$  is the total column concentration of ammonia (molecules  $\text{cm}^{-2}$ ), measured by satellite remote sensors,  $T_{soil}$  is the soil temperature at the surface, which can be expressed as the skin temperature,  $T_{skin}$  (Kelvin),  $a$  and  $b$  are constants ( $a = 2.75 \times 10^3 \text{ g K cm}^{-3}$ ,  $b = 1.04 \times 10^4 \text{ K}$ ),  $M_{\text{NH}_3}$  is the molar mass of ammonia gas ( $M = 17.031 \text{ g mol}^{-1}$ ), and  $N_a$  is Avogadro's number ( $N_a = 6.0221409 \times 10^{23} \text{ molecules mol}^{-1}$ ),  $c'$  is equals to 100 and is added to convert  $k$  from  $\text{m s}^{-1}$  to  $\text{cm s}^{-1}$  (since  $[\text{NH}_3]^{col}$  is in molecules  $\text{cm}^{-2}$ ), and  $\tau$  the lifetime of ammonia (seconds).

$k$  is the soil – atmosphere exchange coefficient or deposition velocity ( $\text{cm s}^{-1}$ ), also known as the mass transfer coefficient (this nomenclature will be used in this study). It is found to be affected by a function of the roughness length of the surface, wind speed, the boundary layer height (Olesen and Sommer, 1993; Van Der Molen et al., 1990), and pH (Lee et al., 2020). It can also be explained calculated using by a resistance model, often used to explain the exchange between the surface and the atmosphere (Wentworth et al., 2014). Different studies provide look up tables values of  $k$  for different land cover types and different seasons based on this resistance model (Aneja et al., 1986; Erisman et al., 1994; Phillips et al., 2004; Roelle and Aneja, 2005; Svensson and Ferm, 1993; Wesely, 1989).

In general, the mass transfer coefficient  $k$  is in the order of  $10^{-3}$  to  $10^{-2} \text{ m s}^{-1}$  in a mixture of soil and manure, and  $10^{-6}$  to  $10^{-5} \text{ m s}^{-1}$  in a mixture of manure alone (Roelle and Aneja, 2005). We discuss and provide more information on  $k$  in Sect. 3.24, and additional details on this calculation in general are provided in Appendix A.

### 2.2. IASI ammonia, ERA5 T skin, and MODIS Land cover

The Infrared Atmospheric Sounding Interferometer (IASI) is considered advanced the most innovative instrument onboard the polar-orbiting Metop satellites (Klaes, 2018). Three IASI instruments are onboard Metop-A, B and C, the series of satellites launched by the EUMETSAT (European Organization for the Exploitation of Meteorological Satellites) in 2006, 2012, and 2018, respectively. The Metop-A satellite was de-orbited in October 2021 (Lentze, 2021), and as a result only two

instruments (IASI-B and C onboard Metop-B and C) are operating today. [The observations from IASI IASI's observations](#) cover any location on Earth at 9:30 in the morning (AM) and in the evening (PM), local solar time. It can detect a variety of atmospheric species including trace gases (Clerbaux et al., 2009). The IASI Fourier-transform spectrometer monitors the atmosphere in the spectral range between 645 and 2760  $\text{cm}^{-1}$  (thermal infrared), and is nadir-looking. [IASI has a swath width that The width of IASI's swath](#) measures 2200 km, with a pixel size of  $\sim 12$  km.

Ammonia was first detected with IASI using the  $\nu_2$  vibrational band of ammonia ( $\sim 950 \text{ cm}^{-1}$ ) (Clerbaux et al., 2009; Coheur et al., 2009). The ammonia total columns used in this study are the product of an Artificial Neural Network and re-analyzed temperature data from the European Centre for Medium-Range Weather Forecasts (ECMWF) product ERA5 ANNI-NH<sub>3</sub>-v3R-ERA5 (Van Damme et al., 2021). Several studies used ammonia data from IASI to study hotspots of ammonia of different source types including both natural and anthropogenic sources (Clarisse, Van Damme, Clerbaux, et al., 2019; Clarisse, Van Damme, Gardner, et al., 2019; Dammers et al., 2019; Van Damme et al., 2018, 2021; Viatte et al., 2021). Recently, IASI observations were used to study the effect of war and conflict on agricultural practices in Syria (Abeed et al., 2021).

Fewer errors on the retrieval were observed during the day and over land (Van Damme et al., 2017), hence, we use only daytime ammonia measurements from IASI. Comparisons with ammonia measured using a ground-based instrument showed a good correlation of  $R=0.75$  (Viatte et al., 2021). Satellite ammonia data from CrIS (Crosstrack Infrared Sounder) (Shephard and Cady-Pereira, 2015) were compared with those from IASI, and were equally found to give similar results when looking at concentrations from a wildfire (Adams et al., 2019), showing consistency when studying seasonal and inter-annual variability (Viatte et al., 2020).

In addition to ammonia, we look at skin temperature (T skin or land surface temperature LST) data from the ECMWF's reanalysis (ERA5) at a grid resolution of  $0.25 \times 0.25^\circ$  (Hersbach et al., 2020). ERA5 Temperatures are interpolated temporally and spatially to the IASI morning overpass ( $\sim 9:30$  A.M. local time), since we only consider daytime ammonia. ERA5 temperature data are also used in the retrieval process of the ammonia data we used in this study NH<sub>3</sub>-v3R-ERA5 (Van Damme et al., 2021). T skin is defined as the temperature of the uppermost surface layer when radiative equilibrium is reached. It also represents the theoretical temperature required in order to reach the surface energy balance (ECMWF, 2016). [Skin temperature in Europe varies with a standard deviation on the daily average that is mostly between 2 and 6°C, in Northern, Central, Western and South-western Europe. And between 4 to 8°C in Eastern Europe \(not shown here\).](#)

In order to assign a mass transfer coefficient  $k$  to each land type, the moderate resolution imaging spectroradiometer (MODIS), a series of instruments orbiting the Earth aboard the Aqua and Terra satellites, is used. The data product MCD12Q1 (version 6) is a combined Aqua/Terra Land cover type product, with a spatial resolution of 500 m. This product provides maps of land cover type from 2001 through 2019 (Sulla-Menashe and Friedl, 2018). From the land use categories included in the MOD12Q1 product (Belward et al., 1999) we focus on croplands, forests, shrublands, and grasslands. We do not include barelands, snow cover, and urban areas in our analysis; we are not interested in studying these surfaces, since we focus on ammonia volatilization from the soil in areas ~~amended-where~~ [fertilizers are applied. In addition to croplands, in this study we show](#) ~~We show~~ the emission potential in ~~f~~Forests and grasslands/shrublands for comparison with values in the literature. In an attempt to calculate an emission potential (Eq. ~~(2-1)(2-4)~~) that is relevant to the land cover/use, we therefore assign a mass transfer coefficient  $k$  to each land type based on literature values (Aneja et al., 1986; Erisman et al., 1994; Roelle and Aneja, 2005; Svensson and Ferm, 1993; Wesely, 1989) and we discuss it in Sect. [3.24](#).

## 2.3. Model simulations

### 2.3.1. GEOS-Chem Chemistry Transport Model

In this study we use version 12.7.2 of the GEOS-Chem chemical transport model (Bey et al., 2001). The model is driven by the Modern-Era Retrospective Analysis for Research and Applications version 2 (MERRA-2) reanalysis product, including nested domains over Europe at a  $0.5^\circ \times 0.625^\circ$  horizontal resolution. MERRA-2 is the second version of the MERRA atmospheric reanalysis product by NASA's Global Modulation Assimilation Office (NASA/GMAO) (Gelaro et al., 2017). Boundary conditions for the nested domains are created using a global simulation for the same months at  $2^\circ \times 2.5^\circ$  resolution. We generate model output for March of 2011, preceded by a one month of discarded model spin-up time for the nested run, and two months for the global simulation. March corresponds well [to the month of fertilizer application in Europe, and as](#)

202 ~~such to~~ the beginning of the growing season (FAO, 2022; USDA, 2022), ~~and as such to the month of fertilizers application in~~  
203 ~~Europe.~~

204  
205 Output includes the ~~hourly monthly~~-mean for selected diagnostics. Anthropogenic emissions are taken primarily from the global  
206 Community Emissions Data System (CEDS) inventory (Hoesly et al., 2018). Biogenic non-agricultural ammonia, as well as  
207 ocean ammonia sources, are taken from the Global Emission Inventories Activities database (GEIA, (Bouwman et al., 1997)).  
208 Open fire emissions are generated using the GFED 4.1s inventory (Randerson et al., 2015). We used the Harmonized Emissions  
209 Component module (HEMCO) to obtain the ammonia emissions over Europe (Keller et al., 2014).  
210

### 211 2.3.2. EC-Earth Climate model

212 To analyze how future climate will affect ammonia concentration and emission potential, we use the ECMWF ~~climate model~~  
213 ~~the~~-European Earth Consortium climate model (EC-Earth, <http://www.ec-earth.org/>). While other climate models exist, we  
214 choose this one because ~~the ammonia product from IASI uses IASI's ammonia product uses~~ ERA5 for the retrievals and we  
215 calculate the emission potential from the T skin product of ERA5. The reanalysis uses the ECMWF's Integrated Forecasting  
216 System for the atmosphere-land component (IFS). IFS is also used in EC-Earth and is complemented with other model  
217 components to simulate the full range of Earth system interactions that are relevant to climate (Döscher et al., 2021). We note  
218 that the versions of the IFS models used in ERA5 and in EC-Earth are not identical as the climate model product is not  
219 assimilated and is not initialized with observations several times a day like ERA5. The EC-Earth simulations are included in  
220 the Climate model intercomparison project, phase 6 (Eyring et al., 2016), part of the Intergovernmental Panel on Climate  
221 Change (IPCC) report of 2021 (Masson-Delmotte, et al., 2021). We use the so-called Scenario Model Intercomparison Project  
222 (ScenarioMIP), covering the period [2015 – 2100] for future projections under different shared socio-economic pathways (SSP)  
223 (Riahi et al., 2017). We analyze two scenarios: ~~the SSP2-4.5, a "middle of the road" socio-economic scenario with a nominal~~  
224 ~~4.5 W/m<sup>2</sup> radiative forcing level by 2100, similar to the RCP-4.5 scenario, and the SSP5-8.5, the upper edge of the SSP scenario~~  
225 ~~spectrum with a high fossil-fuel development use over the 21st century, the SSP2-4.5 corresponding to "middle of the road"~~  
226 ~~socio-economic family with a nominal 4.5W/m<sup>2</sup> radiative forcing level by 2100—approximately corresponding to the RCP 4.5~~  
227 ~~scenario, and the SSP5-8.5 marks the upper edge of the SSP scenario spectrum with a high reference scenario in a high fossil-~~  
228 ~~fuel development world throughout the 21st century.~~

## 229 2.—GEOS-Chem model simulation: validation and analysis

### 230 2.5.2.4. GEOS-Chem validation with IASI

231  
232 ~~In order to~~ To analyse how well the model simulates atmospheric ammonia, we ~~use compare~~ the simulated GEOS-Chem ~~monthly~~  
233 ~~hourly~~ averaged (March 2011) ammonia total columns output (Sect. 2.3.12.3.1). ~~We compare those to with~~ the IASI-NH<sub>3</sub> total  
234 columns ~~of ammonia~~-gridded on the same horizontal resolution (0.5° × 0.625°) and ~~over during~~ the same month. ~~We applied~~  
235 ~~temporal coincidence criterion to GEOS-Chem outputs in order to compare them with IASI morning observations. For instance,~~  
236 ~~we selected data between 8:30 and 11:30 UTC in the GEOS-Chem model output.~~

Code de champ modifié

Mis en forme : Expositant

Mis en forme : Indice

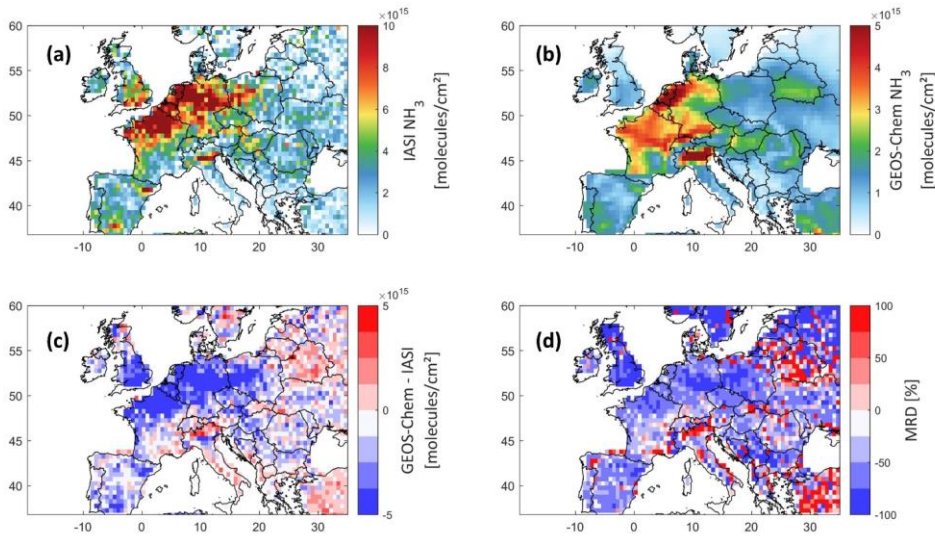


Figure 1. Ammonia total column concentrations from IASI (panel a), and GEOS-Chem (panel b), the difference between both datasets (panel c) in molecules  $\text{cm}^{-2}$ , and the Mean Relative Difference (MRD) in % (panel d); all data are a monthly average of March 2011, and over Europe at a  $0.5^\circ \times 0.625^\circ$  grid resolution. Note that the colour bar limits are different between panels (a) and (b).

237  
238

Figure 1 shows the IASI  $\text{NH}_3$  distribution (Figure 1a), and that from GEOS-Chem (Figure 1b), the bias between the two (Figure 1c), and the mean relative difference MRD (Figure 1d), all during March 2011.

241 MRD is calculated as the mean of the ratio  $\frac{\text{GeosChem NH}_3 - \text{IASI NH}_3}{\text{IASI NH}_3} \times 100$  at each grid point.

242  
243

244 Generally, both GEOS-Chem and IASI show coincident sources of ammonia, reflecting the good ability of the model to reproduce ammonia columns over major agricultural source regions in Europe. The bias between IASI and GEOS-Chem and the mean relative difference (MRD) are shown in Figure 1c and d. Ammonia columns from GEOS-Chem are underestimated by up to  $2 \times 10^{16}$  molecules/ $\text{cm}^2$  in some source regions, especially in England, North Eastern France, the North European Plain (Netherlands, Belgium), and Spain (around Barcelona). Similar results were found in the study of Whitburn et al. (2016), in which they show that GEOS-Chem underestimates ammonia columns by up to  $1 \times 10^{16}$  molecules/ $\text{cm}^2$  in Europe on a yearly average in 2009, notably in the North European Plain. It is important to note that, in our study, we compare only one month of data (March, 2011) that which marks the start of the growing season in the majority of the countries of interest (FAO, 2022; USDA, 2022). (Ageste, 2014) (Einarsson et al., 2021) The differences are most likely due to the fact that, with IASI, cloud-free data are used to retrieve ammonia mainly because of the time coincidence, and the fact that only cloud-free data are used to retrieve ammonia; IASI observes ammonia during the satellite overpass (~9:30 AM local time), whereas the GEOS-Chem simulation is averaged over the whole month including all hours of the day. In most of the studied regions, Western and Northern Europe, the MRD is around mostly less than -50% ( $\pm 7\%$  in absolute value, for instance, in Brittany MRD = -43%, whereas in both Barcelona and Valladolid in Spain, it is -57%. While in the North European Plain (-49%). If we look at the average MRD in regions of focus, we see that the Po Valley in Italy/England y shows the highest MRD value in absolute terms (-79%) (-110%), whereas the best represented region is the Po Valley

259

Code de champ modifié

Mis en forme : Couleur de police : Automatique, Non Surlignage

260 (+0.1 %), then follows the region of New Aquitaine in the southwest of France (-34.120 %) (see Table 1). The rest of the  
261 regions have mean MRDs that fluctuate between -64 % and -42 %. A summary of the results of this study, including the  
262 MRD over some source regions is listed in Table 1. Although the biases and MRD values can be considered as high,  
263 the spatial distribution is consistent between IASI and GEOS-Chem. Therefore, according to the steady-state approximation,  
264 the we assume that meteorological and soil parameters affecting one dataset (e.g. IASI NH<sub>3</sub>) are applicable to the other (e.g.  
265 model simulation), this is known as the steady-state approximation. It is worth noting that although we do not use the latest  
266 version of GEOS-Chem, the results we obtain reflects our current understanding of the regional chemistry at this horizontal  
267 and temporal resolution.

268 The frequency of fertilizers application can vary per crop type and per country, as well as from year to year. In Europe, however,  
269 the N applied per surface area is quite stabilized after year 1980, with some interannual fluctuations in most European countries  
270 (Einarsson et al., 2021). As to our knowledge, accurate information on the application frequency per country is not reported.  
271 While the application frequency can change from year to year, the fluctuations are less pronounced after the year 2000. For  
272 instance, in France and Belgium the nitrogen content fluctuates between 100 and 110 kg N/ha/year, from 2000 to 2020  
273 (Einarsson et al., 2021).

### 276 3. Results and discussions

#### 277 2.6.3.1. Ammonia emissions, losses and lifetime in Europe

278 In order to understand the NH<sub>3</sub> spatial variability in Europe during the application of fertilizers, a detailed analysis of the output  
279 of the GEOS-Chem simulation for the month of March 2011 is shown in Figure 2.

280 The anthropogenic sources (i.e. mainly agriculture) contribute 83 % of the total ammonia emissions during March 2011 in  
281 Europe. The ammonia emissions from natural sources (i.e. soil of natural vegetation, oceans, and wild animals) follow  
282 representing 16 % of the total emissions, whereas the remaining 1 % correspond to the ammonia emissions from biomass  
283 burning and ships (not shown here).

284 Figure 2a shows the monthly ammonia emissions of ammonia. Most of these emissions are due to  
285 agricultural activities (not shown here); we identify 8 source regions which we investigate thoroughly in this study shown as  
286 rectangles A to H. The highest agricultural sources over Europe include the North European Plain, Brittany, and the Po Valley  
287 (regions C, D, and F).

288 In the calculation of the total loss of ammonia (Figure 2b), we considered dry deposition, chemistry, transport, and wet  
289 deposition (in which we included ammonia loss to convection) from the GEOS-Chem model simulation, which are all possible  
290 loss processes for ammonia (David et al., 2009). Figure 2b shows that the largest losses occur logically where we have  
291 the highest sources detected (see Figure 2a).

292  
293

Code de champ modifié

Mis en forme : Police de script complexe :10 pt

Mis en forme : Non Surlignage

Mis en forme : Non Surlignage

Mis en forme : Non Surlignage

Mis en forme : Non Surlignage

Mis en forme : Non Surlignage

Mis en forme : Non Surlignage

Mis en forme : Non Surlignage

Mis en forme : Non Surlignage

Mis en forme : Titre 1, Espace Avant : 20 pt, Après : 6 pt, Hiérarchisation + Niveau : 1 + Style de numérotation : 1, 2, 3, ... + Commencer à : 1 + Alignement : Gauche + Alignement : 0 cm + Retrait : 0,63 cm, Lignes solitaires

Mis en forme : Police : (Par défaut) + Titres CS (Times New Roman), Police de script complexe : + Titres CS (Times New Roman), 10 pt

Mis en forme : Police : (Par défaut) + Titres CS (Times New Roman), Police de script complexe : + Titres CS (Times New Roman), 10 pt

Mis en forme : Police : (Par défaut) + Titres CS (Times New Roman), Police de script complexe : + Titres CS (Times New Roman), 10 pt

Mis en forme : Police : (Par défaut) + Titres CS (Times New Roman), Police de script complexe : + Titres CS (Times New Roman), 10 pt

Mis en forme : Police : (Par défaut) + Titres CS (Times New Roman), Police de script complexe : + Titres CS (Times New Roman), 10 pt

Mis en forme : Police : (Par défaut) + Titres CS (Times New Roman), Police de script complexe : + Titres CS (Times New Roman), 10 pt

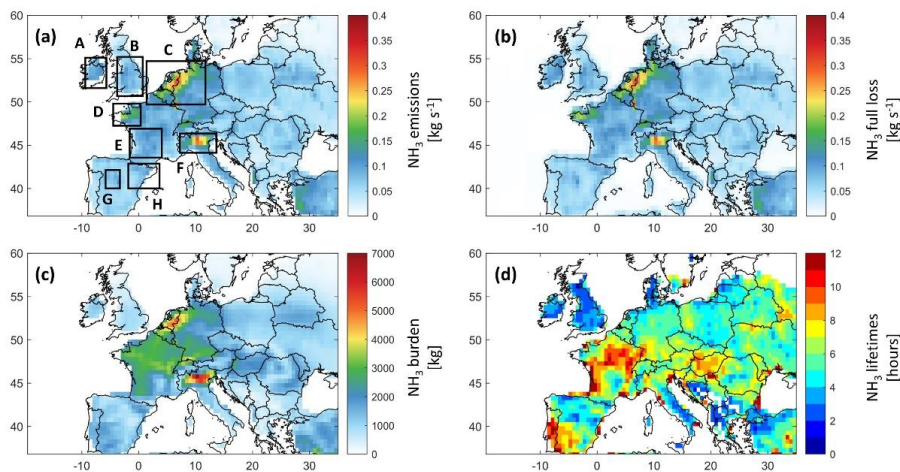


**Figure 2. Ammonia budget in Europe from GEOS-Chem: (a) Ammonia emissions from the Harmonized Emissions Component module (HEMCO) in  $\text{kg s}^{-1}$  with our regions of interest shown in rectangles, (b) ammonia full loss in  $\text{kg s}^{-1}$ , (c) ammonia total burden in kg, and (d) ammonia lifetime in hours. All plots refer to March 2011 and are presented at a  $0.5^\circ \times 0.625^\circ$  grid resolution.**

The total ammonia burden (Figure 2c) is calculated as the integrated sum of all ammonia columns in the model grid box. We can clearly detect ammonia hotspots over Europe, in particular the North European Plain, Brittany and the Po Valley, all regions characterized by intense agricultural activities, as the total emissions and deposition show (Figure 1 and Figure 2). We also see that the burden is generally the highest over France, Belgium, The Netherlands, and parts of Germany and Italy.

The lifetime  $\tau_{ss}$  of ammonia is shown in (Figure 2d). In the case of a gas with a short lifetime, such as ammonia, the emissions are relatively well-balanced spatially by eventual sinks/losses (steady-state approximation). Therefore, we can calculate a steady-state lifetime as the ratio between the total burden  $B$  (Figure 2c) and the total emissions  $E$  or losses  $L$  (sum of all emitted / lost molecules, Figure 2a or b) using the following equation:  $\tau_{ss} = B/L$  (Plumb and Stolarski, 2013).

We note that the  $\tau_{ss}$  is more or less the same whether we calculate it using the losses or the emissions. For instance, in selected source regions (rectangles in Figure 2a) the total emissions and losses are very close with very low biases that are less than 2% (not shown here). Our results show that  $\tau_{ss}$ , on a monthly average, can go up to 12 hours, and it can reach 1 day (24 hours) in coastal regions such as region E in New Aquitaine in France. The latter can be related to the high probability of air stagnation in that area, especially during spring, in comparison to Northern Europe (Garrido-Perez et al., 2018), since higher  $\text{PM}_{2.5}$  pollution episodes were found under stagnant meteorological conditions (AQEG, 2012); and these  $\text{PM}_{2.5}$  particles can dissociate, releasing ammonium molecules carried on these  $\text{PM}_{2.5}$  can transform back into ammonia. Our results agree with the literature suggesting a residence time between a few hours to a few days (Behera et al., 2013; Pinder et al., 2008). We note that, and with those calculated by Evangeliou et al. (2021) estimated the lifetime of ammonia over Europe using a different model and; the results showing showed a monthly average of ammonia lifetime that ranges from 10 to 13 hours in Europe. The figure adapted from Evangeliou et al. (2021) is shown in supplementary material (Figure S1). Shorter lifetimes from industrial sources of ammonia were reported in Dammers et al. (2019), with a mean lifetime of ammonia that is equal to 2.35 hours ( $\pm 1.16$ ). A recent study found lifetimes of ammonia that vary between 5 and 25 hours, roughly, in Europe (Luo et al., 2022); these values are higher since, in addition to ammonia loss, Luo et al. (2022) included the loss of ammonium, and thus considering the loss of ammonia only terminal when the ammonium is also lost/deposited. This approach is not considered adopted here nor in Evangeliou et al. (2021).

Mis en forme : Police : (Par défaut) +Titres CS (Times New Roman), Police de script complexe : +Titres CS (Times New Roman), 10 pt

Mis en forme : Police : (Par défaut) +Titres CS (Times New Roman), Police de script complexe : +Titres CS (Times New Roman), 10 pt

Mis en forme : Police : (Par défaut) +Titres CS (Times New Roman), Police de script complexe : +Titres CS (Times New Roman), 10 pt

Mis en forme : Police : (Par défaut) +Titres CS (Times New Roman), Police de script complexe : +Titres CS (Times New Roman), 10 pt

Mis en forme : Police : (Par défaut) +Titres CS (Times New Roman), Police de script complexe : +Titres CS (Times New Roman), 10 pt

Mis en forme : Police : (Par défaut) +Titres CS (Times New Roman), Police de script complexe : +Titres CS (Times New Roman), 10 pt

Mis en forme : Indice



323 Notably, ammonia lifetime and burden (Figure 2c, and d) each have different spatial distribution compared to the other  
 324 2 panels (Figure 2a, and b). The ammonia residence time in the atmosphere varies depending on the sources and more  
 325 importantly on the locally dominant loss mechanisms. For this reason, in Figure 3, we show the relative contribution  
 326 of the ammonia loss mechanisms, presented as pie charts, for the agricultural source regions shown in black boxes in Figure  
 327 2a.

328  
 329 The fastest loss mechanisms are either chemical (i.e. in the vast majority transformation to particulate matter) or through wet  
 330 and dry deposition (Tournadre et al., 2020). Figure 3 shows that more than 50 % of the ammonia molecules in the  
 331 atmosphere are lost to chemical reactions in most of the regions (A, B, C, H, and F). The shortest residence time of ammonia  
 332 is observed in England, where the chemical removal was significantly higher than other sinks and represented up to 73 % of  
 333 the total ammonia loss pathways, suggesting a rapid transformation into inorganic particulate matter (PM<sub>2.5</sub>). In the regions D,  
 334 G and E the chemical loss makes up 50 %, 49 %, and 42 %, respectively. In fact, in March 2011, PM was found to be mostly  
 335 composed of inorganic nitrate (41 %), and ammonium (20 %) (Viatte et al., 2022) over Europe, both of which are products of  
 336 atmospheric ammonia. Nitrate-bearing PM<sub>2.5</sub> are formed when nitric acid (HNO<sub>3</sub>) reacts with ammonia (Yang et al., 2022), and  
 337 ammonium is a direct product of the hydrolysis of ammonia. 41% of the nitric acid formed in the atmosphere is produced from  
 338 the reaction between nitrogen dioxide (NO<sub>2</sub>) and the hydroxyl radical (OH) (Alexander et al., 2020). These chemical pathways  
 339 help explain the large chemical losses in most of the regions studied in Figure 3.

340  
 341 Ammonia loss to transport is the highest in regions neighbouring the Atlantic Ocean, accounting for 30 %, 27 %, 32 %, and 34  
 342 % of total sinks in regions A, D, E, and G respectively. These regions are exposed to the North Atlantic Drift, also known as  
 343 the Gulf Stream, that is associated with high wind speed and cyclonic activity (Barnes et al., 2022). Although the gulf stream  
 344 also affects the loss to transport in England (region B), the chemical loss is the dominant one. Acids, such as HNO<sub>3</sub> and H<sub>2</sub>SO<sub>4</sub>  
 345 react with ammonia in the atmosphere. Therefore, high atmospheric concentrations of NO<sub>2</sub> and SO<sub>2</sub> (from which HNO<sub>3</sub> and  
 346 H<sub>2</sub>SO<sub>4</sub> are derived respectively), induce higher loss of ammonia to chemical reactions. In England, the annual concentration  
 347 mean of both NO<sub>2</sub> and SO<sub>2</sub> are higher than in Ireland (European Environment Agency, 2017a, 2017b). This can explain why  
 348 the largest proportion of NH<sub>3</sub> is lost to chemistry in England, in spite of the effect of the gulf stream. In other regions, 14 % to  
 349 22 % of the total ammonia is lost to transport mechanisms, and in all regions, 11 to 22 % is lost to dry deposition (Figure

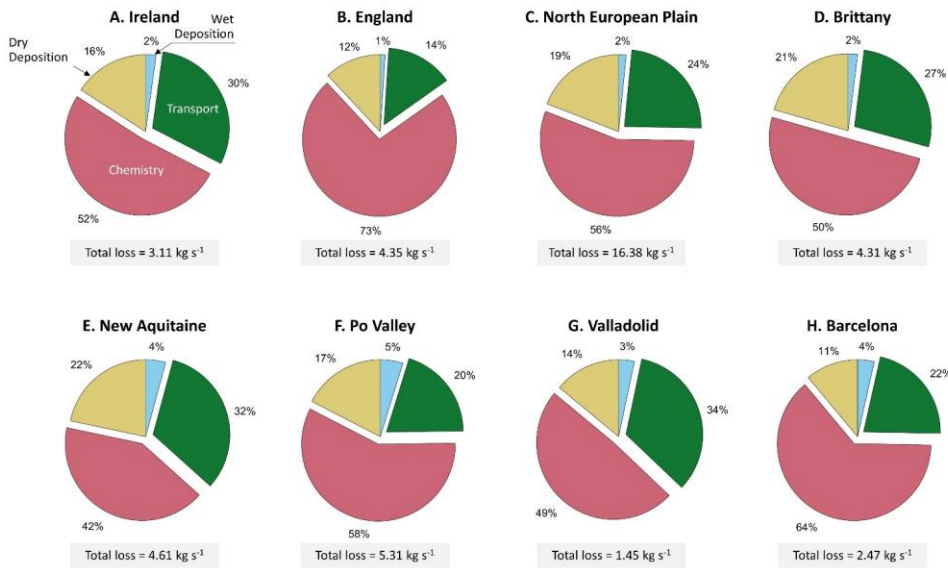


Figure 3. Repartition of the ammonia loss mechanisms for major agricultural areas in Europe, during March 2011, as retrieved from GEOS-Chem, with the total ammonia loss shown in a grey box under each pie chart (kg s<sup>-1</sup>). The regions are shown in black boxes in Figure 2a.

Mis en forme : Police : (Par défaut) +Titres CS (Times New Roman), Police de script complexe : +Titres CS (Times New Roman), 10 pt

Mis en forme : Police : (Par défaut) +Titres CS (Times New Roman), Police de script complexe : +Titres CS (Times New Roman), 10 pt

Mis en forme : Police : (Par défaut) +Titres CS (Times New Roman), Police de script complexe : +Titres CS (Times New Roman), 10 pt

Mis en forme : Police : (Par défaut) +Titres CS (Times New Roman), Police de script complexe : +Titres CS (Times New Roman), 10 pt

Mis en forme : Police : (Par défaut) +Titres CS (Times New Roman), Police de script complexe : +Titres CS (Times New Roman), 10 pt

Mis en forme : Police : (Par défaut) +Titres CS (Times New Roman), Police de script complexe : +Titres CS (Times New Roman), 10 pt

Mis en forme : Couleur de police : Automatique

Mis en forme : Police : (Par défaut) +Titres CS (Times New Roman), Police de script complexe : +Titres CS (Times New Roman), 10 pt

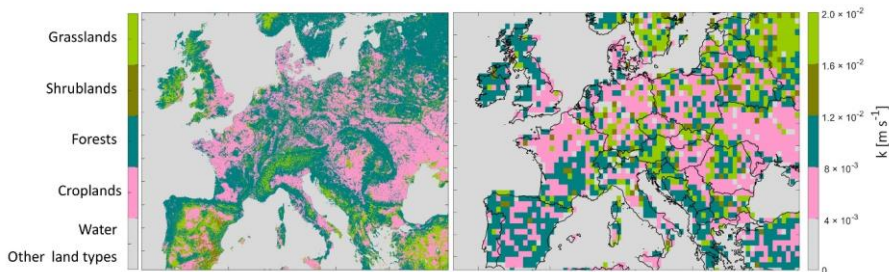
350 **Figure 3**). During March, precipitation is relatively lower as compared to winter (December, January, February) in Europe.  
 351 Furthermore, 2011 was a particular dry year compared to the 1981 – 2010 average (Met Office, 2016). Drought was reported  
 352 to be severe in areas such as France, Belgium and the Netherlands, and moderate in England and Ireland (EDO, 2011). This  
 353 can help explain the low percentage of wet deposition during March 2011 (1 to 5 % out of the total loss of ammonia).  
 354

### 3.3.2. Ammonia emission potential over Europe

355 To calculate emission potential, a calculation of the mass transfer coefficient  $k$ , which relates to the land type, is necessary.  
 356 **Figure 4** shows the land cover type from MODIS in Europe (left panel), and the corresponding assigned mass transfer  
 357 coefficient  $k$  (right panel) needed to calculate the emission potential (Eq. (2-1)-(2-4)). In order to choose a mass transfer  
 358 coefficient that is convenient for the different land types relevant to this study, we searched for  $k$  values in the literature. **Note**  
 359 **that ammonia transfer coefficients are not available for all land types. Not all land types have been studied for ammonia transfer**  
 360 **coefficient.**

361 For water bodies and other land types that are not considered here (see Sect. 2.2.2), the mass transfer values  $k$  were set to zero  
 362 and represented in grey colour in **Figure 4**. In a laboratory experiment, Svensson et al. (1993) reported  $k = 4.3 \times 10^{-3}$   
 363  $\text{m s}^{-1}$  for a mixture of soil and swine manure, as therefore, **therefore, this value was assigned we assign this value to croplands.**  
 364 Due to the lack of  $\text{NH}_3$   $k$  values for non-fertilized forests, shrublands and grasslands in the literature, we used values originally  
 365 assigned for  $\text{SO}_2$ , bearing in mind that these are approximate values and they reflect mostly the conditions of the soil cover  
 366 type (short, medium or tall grass) **rather than the gas itself. In Aneja et al. (1986)(Aneja et al., 1986), the authors estimated the**  
 367 **mass transfer coefficient for both  $\text{NH}_3$  and  $\text{SO}_2$  above different types of crops, they found similar values. For  $\text{NH}_3$ ,  $k$  varied**  
 368 **between 0.3 and 1.3  $\text{cm s}^{-1}$ , and for  $\text{SO}_2$  it varied between 0.5 and 1.5  $\text{cm s}^{-1}$  (Aneja et al., 1986). Since the latter study estimates**  
 369 **several values for  $\text{NH}_3$  mass transfer coefficient, over different types of crops, we will use the  $k$  provided by Svensson et al.**  
 370 **(1993), since it is better adapted to reflect  $\text{NH}_3$  emission from fertilizers, and is not dependent on the crop type. To assign a  $k$**   
 371 **value for forests, we used values reported in Aneja (1986) ( $k = 2 \times 10^{-2} \text{ m s}^{-1}$ ), which originally represent deposition velocity**  
 372 **(mass transfer) of  $\text{SO}_2$  in a forest (high crops), since both  $\text{SO}_2$  and  $\text{NH}_3$  showed similar  $k$  in above crops. For shrublands and**  
 373 **grasslands (the two land types have the same  $k$ ), we used the value  $k = 8 \times 10^{-3} \text{ m s}^{-1}$  that has been reported in Aneja et al.**  
 374 **(1986) as the deposition velocity (mass transfer) of  $\text{SO}_2$  in a grassland (medium crops). These values obtained by using MODIS**  
 375 **land cover types and published estimates of  $k$  values**  
 376 **represent our best effort to realistic mass transfer coefficients, and therefore realistic soil emission potentials. These values are**  
 377 **the best attempt to test the validity of using MODIS and lookup tables of  $k$  values to calculate a realistic soil emission potential.**  
 378 **As a result, Figure 4 (left panel) includes 5 land types, while  $k$  values are reported for 4 land types (other land type/water,**  
 379 **croplands, forests, and shrublands/grasslands).**

380 After choosing the  $k$  values, we assigned them for each land type on the (500 m  $\times$  500 m) grid. We then **extrapolate-aggregate**  
 381 the array with the  $k$  values from 500 m  $\times$  500 m to the resolution of GEOS-Chem (0.5°  $\times$  0.625° grid box). This leads to  
 382 averaging different fine pixels with different land cover types into a coarser grid. The result is shown on the right panel of  
 383 **Figure 4**.  
 384



Mis en forme

Mis en forme : Police : (Par défaut) + Titres CS (Times New Roman), Police de script complexe : + Titres CS (Times New Roman), 10 pt

Mis en forme : Police : (Par défaut) + Titres CS (Times New Roman), Police de script complexe : + Titres CS (Times New Roman), 10 pt

Mis en forme : Indice

Mis en forme : Indice, Non Surlignage

Mis en forme : Indice, Non Surlignage

Mis en forme : Indice, Non Surlignage

Mis en forme : Exosant

Mis en forme : Indice, Non Surlignage

Mis en forme : Exosant, Non Surlignage

Mis en forme : Non Exosant/ Indice, Non Surlignage

Mis en forme : Indice, Non Surlignage

Mis en forme : Indice

Mis en forme : Indice, Non Surlignage

Mis en forme : Indice, Non Surlignage

Mis en forme : Police : (Par défaut) + Titres CS (Times New Roman), Police de script complexe : + Titres CS (Times New Roman), 10 pt

389  
390  
391  
392  
393  
394  
395  
396  
397  
398  
399  
400  
401  
402

Uncertainties of this methodological approach can be summarized as follows:

- (1) The  $k$  value assigned for croplands is approximate and therefore not the same in every cropland over Europe.
- (2) The  $k$  value assigned for forests represents the  $\text{SO}_2$  exchange in high croplands; this value may be very different for ammonia, since  $\text{NH}_3$  can easily dissolve in the water film on leaves under conditions of high humidity.
- (2) The  $k$  value assigned for forests represents the  $\text{SO}_2$  exchange in high croplands, and ammonia might change especially when the latter is highly affected by humidity; it can easily dissolve in the water film on leaves in high humid conditions.
- (3) The extrapolation-While changing the resolution of a fine array ( $500 \text{ m} \times 500 \text{ m}$ ), several grid points will merge several grids together are merged and averaged together them in order to construct the coarser grid box ( $0.5^\circ \times 0.625^\circ$ ); the result is therefore an average that might mix croplands with neighboring forests/barelands/grasslands. This leads to a range of different  $k$  values that are shown on Figure 4.

Using the a land-type specific  $k$  value is necessary in order to reflect realistic emissions potential, we call this the variable  $k$ , as ammonia exchange in a forest is different from that of croplands or unfertilized grasslands, due to different barriers (long,

Figure 4. MODIS Land Cover Type, at a  $500 \text{ m} \times 500 \text{ m}$  grid box (left panel), and interpolated mass transfer coefficient  $k$  (variable

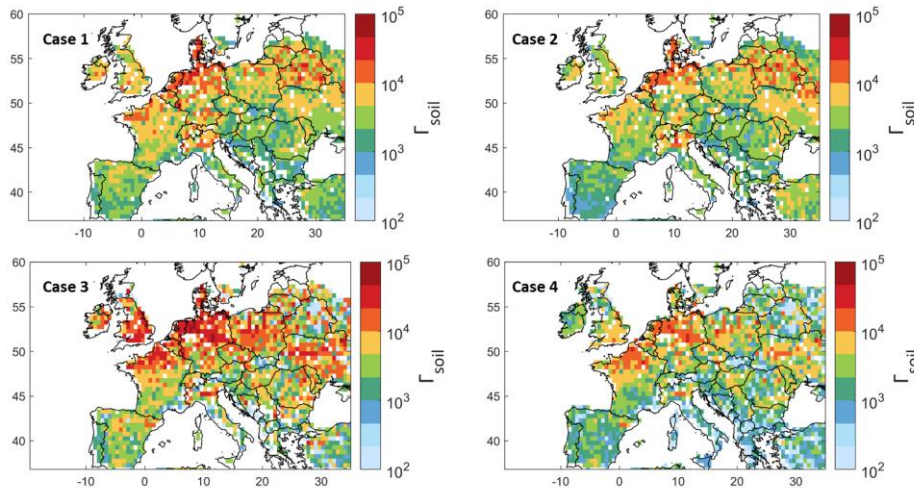


Figure 5. Ammonia soil emission potential ( $\Gamma_{soil}$ ) on a log10 scale from model simulation, observation and reanalysis for 4 different cases (see text for details).

403 medium or short crop / grass), and ammonium soil content in each land type.

404  
405  
406  
407  
408  
409  
410  
411  
412  
413  
414  
415

We show in supplementary material Figure S2, the emission potential (similarly to what we show in Figure 5) but from a fixed and averaged  $k$  value for all land types. Figure S2 shows the importance of using a variable  $k$  that is adjusted to each land type is depicted in supplementary materials (Figure S2). In Figure S2, the fixed  $k$  used is calculated assuming 14 days of fertilization ( $k = 10^{-3} \text{ m s}^{-1}$ ), 7 days when  $k$  value reduces ( $k = 10^{-5} \text{ m s}^{-1}$ ), and 10 days when  $k$  is low ( $k = 10^{-6} \text{ m s}^{-1}$ ) resulting in average of  $k = 4.5 \times 10^{-4} \text{ m s}^{-1}$ . The difference in the emission potential between fixed and spatially variable  $k$  is shown in supplementary material Figure S2, where we see that a fixed  $k$  might overestimate  $\Gamma_{soil}$  by 10 to  $10^3$  on a log10 scale (500–3000%), in agricultural areas.

Figure 5 illustrates the ammonia soil emission potential  $\Gamma_{soil}$  calculated using Eq. (2-1) and  $k$  values presented in Figure 4. After assigning the variable mass transfer coefficient, the remaining variables needed to calculate  $\Gamma_{soil}$  in Eq. (2-1

Mis en forme : Indice

Mis en forme : Police : (Par défaut) +Titres CS (Times New Roman), Police de script complexe : +Titres CS (Times New Roman), 10 pt

Mis en forme : Police : (Par défaut) +Titres CS (Times New Roman), Police de script complexe : +Titres CS (Times New Roman), 10 pt

Mis en forme : Police : (Par défaut) +Titres CS (Times New Roman), Police de script complexe : +Titres CS (Times New Roman), 10 pt, Indice

Mis en forme : Police : (Par défaut) +Titres CS (Times New Roman), Police de script complexe : +Titres CS (Times New Roman), 10 pt

Mis en forme : Police : (Par défaut) +Titres CS (Times New Roman), Police de script complexe : +Titres CS (Times New Roman), 10 pt

Mis en forme : Police de script complexe : +Titres CS (Times New Roman), 10 pt

Mis en forme : Police : (Par défaut) +Titres CS (Times New Roman), Police de script complexe : +Titres CS (Times New Roman), 10 pt

Mis en forme : Normal, Retrait : Avant : 0,63 cm, Sans numérotation ni puces

Mis en forme : Police : (Par défaut) +Titres CS (Times New Roman), Police de script complexe : +Titres CS (Times New Roman), 10 pt

Code de champ modifié

Mis en forme : Police : (Par défaut) +Titres CS (Times New Roman), Police de script complexe : +Titres CS (Times New Roman), 10 pt

416 (2-4) are ammonia concentration and lifetime, as well as the skin temperature. ~~For this reason~~Therefore, the emission potential  
417  $\Gamma_{soil}$  shown in Figure 5 is calculated using different configurations:

- 418
- 419 - Case 1: GEOS-Chem ammonia and lifetime with MERRA-2 T skin, i.e. simulated  $\Gamma_{soil}$ ,
- 420 - Case 2: GEOS-Chem ammonia and lifetime and ERA5 Tskin, to check the effect of using ERA5 vs MERRA-2 for
- 421 skin temperature,
- 422 - Case 3: IASI's ~~NH<sub>3</sub>~~ammonia, ERA5 T skin and GEOS-Chem ammonia lifetime,
- 423 - Case 4: IASI's ammoniaNH<sub>3</sub>, ERA5 T skin and ammonia lifetime from Evangeliou et al. (2021), that were calculated
- 424 using LMDz-OR-INCA chemistry transport model. The latter couples three models: The general circulation model
- 425 GCM (LMDz) (Hourdin et al., 2006), the INteraction with Chemistry and Aerosols (INCA) (Folberth et al., 2006),
- 426 and the land surface dynamical vegetation model (ORCHIDEE) (Krinner et al., 2005).
- 427

428 We show in supplementary material Figure S2, the emission potential (similarly to what we show in Figure 5) but from a fixed  
429 and averaged  $k$  value for all land types. Figure S2 shows the importance of using a variable  $k$  that is adjusted to each land type  
430 is depicted in supplementary materials (Figure S2). In Figure S2, the To calculated a fixed  $k$  (common to all land types) used  
431 is calculated we assume 14 days of fertilization ( $k = 10^{-3} \text{ m s}^{-1}$ , e.g. croplands), 7 days when  $k$  value reduces is reducing  
432 ( $k = 10^{-5} \text{ m s}^{-1}$ ), and 10 days when  $k$  is low ( $k = 10^{-6} \text{ m s}^{-1}$ , e.g. forests) resulting in average of  $k = 4.5 \times 10^{-4} \text{ m s}^{-1}$ . The  
433 difference in the emission potential between fixed and spatially variable  $k$  is shown in supplementary material Figure S3, where  
434 we see that a fixed  $k$  might overestimate  $\Gamma_{soil}$  by 10 to  $10^3$  on a log10 scale (500 – 3000 %), in agricultural areas.

435  
436 ~~Based upon the four cases, we calculate a range of emission potentials.~~When calculating  $\Gamma_{soil}$ , we filtered data points with  
437 ammonia total column concentration less than  $5 \times 10^{14}$  molecules  $\text{cm}^{-2}$ . The latter are mostly grid boxes concentrated above  
438  $56^\circ$  North that we consider as noise (shown in white pixels on Figure 5).

439  
440 T skin from ERA5 and MERRA-2 agree very well, with a coefficient of determination  $r^2 = 0.97$  (Figure S4 in the supplementary  
441 material). This explains the excellent spatial correlation between cases 1 and 2. Note that when using MERRA-2 T skin, we  
442 selected only morning measurements from 8:00 to 10:00 UTC. Since IASI-NH<sub>3</sub> retrievals use ERA5 T skin, this also suggests  
443 that using MERRA-2 or ERA5 does not affect our  $\Gamma_{soil}$  calculation. In case 3, the emission potential agrees spatially ~~and in~~  
444 ~~value~~ with that of GEOS-Chem. However, we observe higher  $\Gamma_{soil}$  in regions such as Ireland, England, Northern France,  
445 Northeastern Spain, and Poland. This is due to the underestimation/~~overestimation~~ of ammonia from GEOS-Chem as compared  
446 to IASI observations (Figure 1a). For instance,  $\Gamma_{soil}$  from IASI and ERA5 (case 3) differs with that from GEOS-Chem  
447 and ERA5 (case 1) by ~~up to 31 % -70 % in the Po Valley (Italy) and +60 % in England Ireland.~~ Looking at ~~Table 1~~Table 1, this  
448 difference can be explained by the corresponding MRD for ~~each Ireland of the regions, in which it is -64.45 % for England~~  
449 ~~and +110 % for the Po Valley. Similarly,~~the differences between case 3 and 4 reach up to ~~+72.66 % in England Ireland,~~  
450 and this is mostly due to the 10-hours difference between ammonia lifetime from GEOS-Chem and Evangeliou et al. (2021) (Figure  
451 S1 in the supplementary material). The lowest  $\Gamma_{soil}$  (in most regions) were obtained in case 4, due to the higher lifetime ~~values~~  
452 ~~from Evangeliou et al. (2021), as compared to those~~ those calculated from GEOS-Chem (Figure S1); note that  $\Gamma_{soil}$  is inversely  
453 proportional to ammonia lifetime (Eq. (2-1)-(2-4)). In fact, the longer ammonia stays in the atmosphere (longer lifetime), the less  
454 the flux will be directed from the soil to the atmosphere (less ammonia emission). We compared  $\Gamma_{soil}$  calculated from all cases  
455 by for each region, and we conclude that cases 2 and 4 showed the best compatibility. For instance,  $\Gamma_{soil}$  from cases 2 and 4  
456 differ by only 6 % in the North European Plain and Brittany, and by 4 % in New Aquitaine. The highest difference between  
457 cases 2 and 4 is observed in the Po Valley (53 %) (not shown here).

458  
459 In the four cases presented in Figure 5, we see similar spatial distribution of ammonia emission potential with values ranging  
460 from  $12 \times 10^{-1}$  in a forest to  $9.5 \times 10^4$  in a cropland (monthly average considering all the cases). In agricultural lands, our results  
461 show that  $\Gamma_{soil}$  ranges from  $2 \times 10^3$  to  $9.5 \times 10^4$ . ~~Our values for croplands start at around  $10^3$ .~~ In fact, most of the studies  
462 summarized in Zhang et al. (2010) reported  $\Gamma_{soil}$  that range mostly from  $10^3$  to  $10^4$  in fertilized croplands/grasslands; the  
463 minimum  $\Gamma_{soil}$  reported is in the order of  $10^2$  and the maximum is of the order of  $10^5$ . Therefore, our values fit within the range  
464 of  $\Gamma_{soil}$  calculated in the literature and summarized in Zhang et al. (2010) and the references within. Personne et al. (2015)  
465 focused on Grignon, an agricultural region near Paris, France ( $48^\circ 51' \text{N}$ ,  $1^\circ 58' \text{E}$ ). They obtained  $\Gamma_{soil}$  values between  $1.1 \times 10^4$   
466 to  $5.8 \times 10^6$ . In the present study, the emission potential over this region is between  $4.5 \times 10^3$  (case 2) to  $2.5 \times 10^4$  (case  
467 24). In this study, lower values than those measured in the field are expected. Therefore, we consider our results to be in good  
468 agreement with the values in Personne et al. (2015), since ours reflect a 31-day mean of an average of over a large area ( $55 \times$   
469  $70 \text{ km}^2$ ) as compared to the localized measurements done by Personne et al. (2015).

Mis en forme : Indice

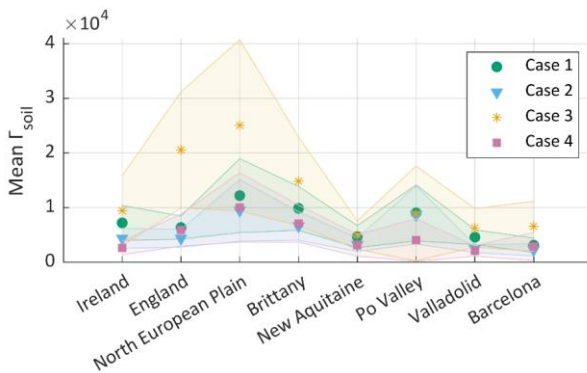
Mis en forme : Non Exposant/ Indice

Mis en forme : Non Exposant/ Indice

Mis en forme : Police de script complexe :10 pt

470 it is expected to obtain lower values than the ones measured over specific field. Therefore, we consider our results to be in good  
 471 agreement with the obtained values in [Personne et al. \(2015\)](#), since ours reflect an average of a coarse patch of land of the size  
 472  $55 \times 70 \text{ km}^2$  approximately, with a 31-day mean.

473  
 474 The mean emission potentials per ammonia source region in Europe (shown in rectangles in [Figure 2](#) and [Figure](#)  
 475 [3](#)) and per case are shown in [Figure 6](#), and listed in [Table 1](#). [Table 1](#) shows the average lifetime  
 476 from GEOS-Chem (hours), the average T skin from the [three-two](#) datasets that we used ( $^{\circ}\text{C}$ ), the average ammonia emission  
 477 potential in all the cases examined (dimensionless), and the average ammonia columns from IASI and GEOS-Chem (molecules  
 478  $\text{cm}^{-2}$ ). The four cases show a similar pattern with the North European Plain exhibiting the highest emission potential. This has  
 479 been shown in [Figure 1](#), [Figure 2](#), and [Figure 5](#), as well as in [Table 1](#), where  $\Gamma_{\text{soil}}$  is higher in regions  
 480 with high ammonia columns. This is expected in fertilized lands (croplands), since  $\Gamma_{\text{soil}}$  is proportional to the concentration of  
 481 ammonia near the surface. The latter increases when the soil content of ammonium ( $\text{NH}_4^+$ ) increases following the application  
 482 of nitrogen-based fertilizers.  
 483



484 **Figure 6.** Mean ammonia emission potential  $\Gamma_{\text{soil}}$  per region and per case, with the error margin on the mean as the shaded area  
 485 (95<sup>th</sup> percentile) for cases 1 to 4. The cases are explained in [the discussion of Figure 5 and its discussion](#).

486 Figure 6 also shows that for cases 1 and 2 (GEOS-Chem) the emission potential in the Po Valley is almost equal higher as  
 487 compared to case 3 (IASI), with  $\Gamma_{\text{soil}} \approx 0.9$  and  $0.86 \times 10^4$  in cases 1 and 2, and  $0.89 \times 10^4$  in case 3 (see [Table 1](#)); although it  
 488 stays within the margin of error. This is due to the effect of temperature. [Table 1](#) shows that at the time of the IASI overpass,  
 489 T-skin from ERA5 in the Po Valley is almost twice as large ( $8.95 \text{ }^{\circ}\text{C}$ ) as the monthly averaged temperature ( $4.46 \text{ }^{\circ}\text{C}$ ). To  
 490 calculate  $\Gamma_{\text{soil}}$  from IASI  $\text{NH}_3$  (case 3 and 4), we used T skin from ERA5 that coincides with the overpass of IASI. We used the  
 491 same T skin values from ERA5 for case 2, as well as hourly concentrations of ammonia from GEOS-Chem (8:30 to 11:30  
 492 UTC). The ERA5 T skin are shown in [Table 1](#). The effect of skin temperature through Eq. (2-1)-(2-4) makes the emission  
 493 potential highly dependent on it. In fact,  $\Gamma_{\text{soil}}$  is both directly and inversely proportional to T skin, however, the exponential in  
 494 the denominator has ~10 times more effect on the value of  $\Gamma_{\text{soil}}$  than the T skin in the numerator. Therefore, through Eq. (2-1)  
 495 (2-4), we conclude that an increase in temperature by  $1^{\circ}\text{C}$  will reduce  $\Gamma_{\text{soil}}$  by around  $-8\%8 \%$ .

496 The standard deviation (shaded area) is found to be the highest in the North European Plain, which is also the largest region  
 497 (hence higher variability is expected), especially when considering case 3 with IASI. IASI distinguishes different source sub-  
 498 regions, leading to higher spatial variability of ammonia, and therefore  $\Gamma_{\text{soil}}$ . As [Figure 5](#) has shown, case 4 has the lowest,  
 499 with a factor of two lower than cases 1 to 3. This is due to the longer lifetimes calculated by [Evangelidou et al. \(2021\)](#). However,  
 500 we note that all the regions exhibit the same inter-variability between each of the case, regardless of the lifetimes used.

Mis en forme : Police : (Par défaut) +Titres CS (Times New Roman), Police de script complexe : +Titres CS (Times New Roman), 10 pt

Mis en forme : Police : (Par défaut) +Titres CS (Times New Roman), Police de script complexe : +Titres CS (Times New Roman), 10 pt

Mis en forme : Police de script complexe : 10 pt

Mis en forme : Police de script complexe : 10 pt

Mis en forme : Police : (Par défaut) +Titres CS (Times New Roman), Police de script complexe : +Titres CS (Times New Roman), 10 pt

Mis en forme : Police de script complexe : 10 pt

Mis en forme : Non Exposant/ Indice

Mis en forme : Couleur de police : Automatique

Mis en forme : Couleur de police : Automatique

Mis en forme : Couleur de police : Automatique

Mis en forme : Couleur de police : Automatique

Mis en forme : Couleur de police : Automatique

Mis en forme : Couleur de police : Automatique

Code de champ modifié

501 Table 1. Summary of ammonia average lifetime, emission potential, concentrations and the T skin in selected  
 502 regions in Europe.

503  
 504  
 505

Region	Country	$\tau_{NH_3}$ [hours]	T skin [°C] $\times 10^4$ [dimensionless]		$\Gamma_{soil} \times 10^4$ [dimensionless]				NH <sub>3</sub> concentrations [molecules $\times 10^{15}$ cm <sup>-2</sup> ]			
			ERA5 IASI Overpass 9:30 UTC ERA5	MERRA-2 8:00 to 10:00 UTC	Case 1	Case 2	Case 3	Case 4	IASI	GEOS- Chem	Mea MRD [%]	
Ireland	Ireland	3.34	8.74 <del>5.78</del>	6.23	0.723	<del>0.440.7</del> 2	0.94	0.26	2.5	<del>1.41.5</del>	- 45.47	Tableau mis en forme
England	England	3.15	8.54 <del>5.87</del>	5.73	0.6382	<del>0.440.7</del> 8	2.06	0.58	4.78	1.2	- 75.79	Mis en forme : Retrait : Avant : 0 cm, Première ligne : 0 cm
North European Plain	Belgium, Netherla nds	5.16	7.46 <del>4.93</del>	4.57	1.8622	<del>0.951.7</del> +	2.51	1.00	7.67	<del>3.53.9</del>	- 55.4	Mis en forme : Retrait : Avant : 0 cm, Première ligne : 0 cm
Brittany	France	6.93	10.48 <del>8.13</del>	8.16	<del>1.190.98</del>	<del>0.661.0</del> 9	1.48	0.70	5.8	3.27	- 43.254	Mis en forme : Retrait : Avant : 0 cm, Première ligne : 0 cm
New Aquitaine	France	8.05	11.25 <del>7.72</del>	7.47	0.4659	<del>0.320.5</del> 7	0.49	0.30	4.0	2.69	- 34.12	Mis en forme : Retrait : Avant : 0 cm, Première ligne : 0 cm
Po Valley	Italy	7.10	8.95 <del>4.46</del>	5.46	<del>1.500.90</del>	<del>0.861.6</del> 3	0.89	0.40	4.0	3.8	+ 0.125	Mis en forme : Retrait : Avant : 0 cm, Première ligne : 0 cm
Valladolid	Spain	4.53	11.64 <del>6.87</del>	6.93	0.5465	<del>0.250.5</del> 5	0.62	0.20	2.5	1.13	- 57.4	Mis en forme : Retrait : Avant : 0 cm, Première ligne : 0 cm
Barcelona	Spain	4.94	12.61 <del>7.05</del>	9.44	<del>0.430.31</del>	<del>0.460.2</del> 5	0.65	0.28	3.2	1.45	- 57.5	Mis en forme : Retrait : Avant : 0 cm, Première ligne : 0 cm

506  
 507  
 508  
 509  
 510  
 511  
 512  
  
 513  
 514

4.3.3. Ammonia under future scenarios: The effect of temperature change on the volatilization of ammonia

Mis en forme

515  
516

517 As seen in Eq. (2-1)-(2-1), higher skin temperatures favour volatilization of ammonia from the soil. In an attempt  
518 to understand how our simplified emission potential model behaves under changing climate, as well as under future  
519 scenarios, we adopt the future T skin simulations from EC-Earth climate model, into Eq. (2-1)-(2-1). The two  
520 climate socio-economic scenarios that we consider are SSP2-4.5 (“middle of the road” scenario where trends  
521 broadly follow their historical patterns), and SSP5-8.5 (a world of rapid and unconstrained growth in economic  
522 output and energy use) (Riahi et al., 2017). The same Figure constructed using  $F_{soil}$  from GEOS-Chem (case 1) is  
523 shown in the supplementary material as Figure S5.

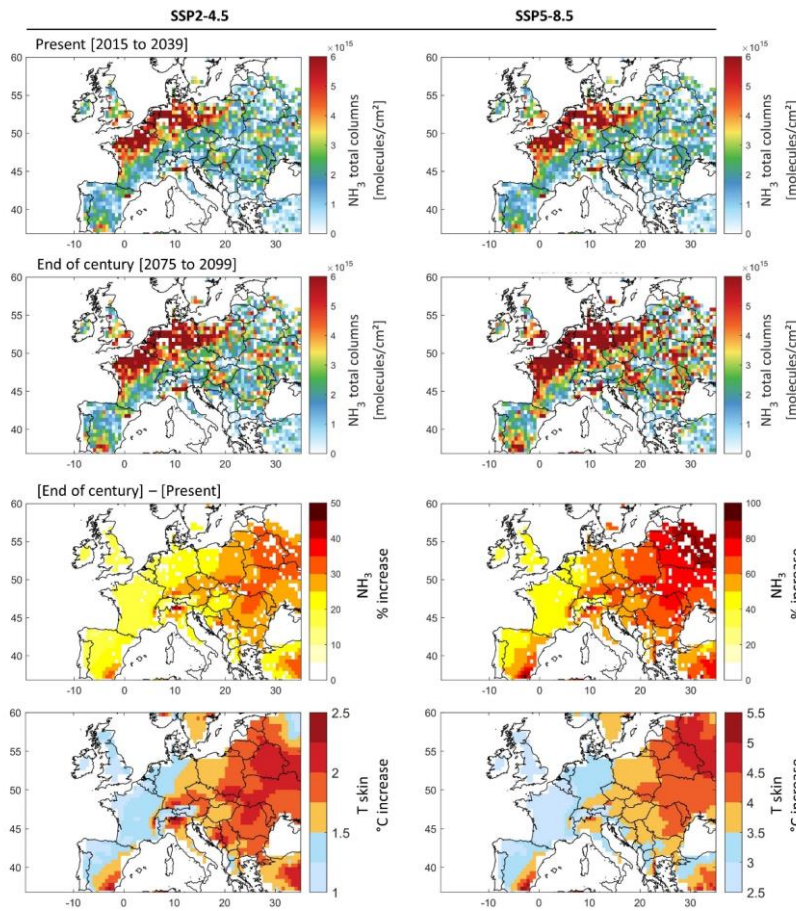


Figure 7. First and second rows: Ammonia total column concentrations during March (monthly averages) under the present climate [2015 to 2039] (first row), and in the end of century climate [2075 to 2099] (second row), under the socio-economic scenarios SSP2-4.5 (left) and SSP5-8.5 (right). Third and fourth rows: The percentage increase in ammonia concentration (third row), and the change in T skin in °C (fourth row) by the end of the century [2075 to 2099] with respect to present climate [2015 to 2039] under SSP2-4.5 (left) and SSP5-8.5 (right). Ammonia columns were calculated using ammonia emission potential  $F_{soil}$  derived from IASI and ERA5 for March 2011 (case 3), and EC-Earth T skin simulations for SSP2-4.5 and SSP5-8.5 extending from 2015 till 2099.

524 We calculate current and future ammonia columns assuming that the emission potential  $F_{soil}$  remains unchanged.  
525 In other words, we assume that the same amount of fertilizers and manure is used until 2100 in the agricultural  
526 fields and farms (unchanged ammonium soil content).

527 **Figure 7** shows ammonia columns during the 25-year [2015 – 2039] representing the present climate  
 528 (upper panels), and the end of the century [2075 – 2099] (middle panels). The ammonia columns in the 25-year  
 529 average climate of the end of century with respect to present day climate (lower panels) are also shown.  
 530

531 Spatially, the present climate ammonia columns calculated from the T skin of the climate model and our emission  
 532 potential from IASI (case 3 in Figure 5), agree very well with those shown in **Figure 1**. We do not aim at  
 533 validating or directly comparing the two, as we are only interested in the climate response on ammonia  
 534 concentration, i.e. by the difference due to skin temperature increase (lower panels).  
 535

536 From **Figure 7** (lower panels) it can be seen that the increase in ammonia columns by the end of the century  
 537 is more severe **on-in-the-eastern-side-of** Europe. Under the most likely scenario (SSP2-4.5), ammonia columns  
 538 vary between +15 % in France, to around +20 % in the North European Plain (**Figure 7**). The largest  
 539 increase is detected in Eastern Europe, where ammonia columns show an increase of up to a +50 % (**Figure 7**  
 540 **7**, lower left panels), creating new potential hotspots/sources of ammonia in Belarus, Ukraine, Hungary, Moldova,  
 541 parts of Romania and Switzerland. Under the SSP5-8.5 scenario, the results show an increase in ammonia columns  
 542 of up to +100 % in Eastern Europe (**Figure 7**, right lower panel). This is directly related to the higher  
 543 projected increase in skin temperature over these regions. Other studies have equally reported Eastern Europe to  
 544 be more affected by climate change under future scenarios, as compared to western Europe (European  
 545 Environment **EnergyAgency**, 2022; Jacob et al., 2018). Spatially, the increase in ammonia coincides with the  
 546 increase in T skin.

547 **Figure 8** depicts the change in ammonia columns under the SSP2-4.5 and SSP5-8.5 scenarios, for our  
 548 source regions (shown as rectangles in **Figure 2**). Ammonia columns increase is foreseen to be the highest  
 549 in the Po Valley (Italy) with +26 % and +59 % under SSP2-4.5 and SSP5-8.5 respectively. It is then followed by  
 550 the agricultural areas around Barcelona (Spain), and the North European Plain (Belgium, Netherlands) with an  
 551 increase of +21 % (+49 %) and +20 % (+53 %) respectively, under the SSP2-4.5 (SSP5-8.5) scenario. Under the  
 552 SSP5-8.5, the increase in ammonia columns in percentage is more than twice the change under SSP2-4.5 (+127 %  
 553 in the case of the Po Valley for instance). The Po Valley is adjacent to the Alps mountains, and due to global  
 554 warming, this region is expected to experience increased evapotranspiration (Donnelly et al., 2017), which is a  
 555 major factor that leads to the volatilization of ammonia.

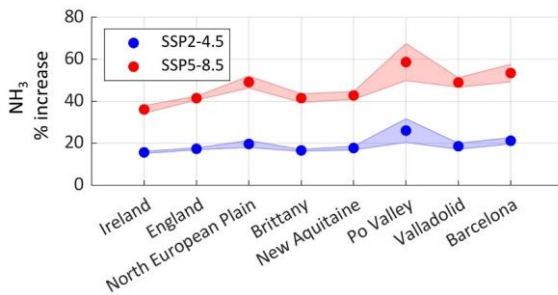


**Figure 8.** The percentage increase in ammonia concentration by the end of the century [2075 to 2099] with respect to the present climate [2015 to 2039] under the two climate scenarios SSP2-4.5 (blue) and SSP5-8.5 (red), in the source regions investigated in this study. The shades around each line represent the standard deviation from the mean.

556 The local and regional effect of volatilization of ammonia under different climate scenarios remains difficult to be  
 557 properly assessed. Even under the “middle of the road” scenario 2-4.5, and without climate extremes (e.g.  
 558 heatwaves), Europe might be facing big challenges in air **quality for regions nearby** or downwind agricultural  
 559 regions, since chemistry and atmospheric transport (**Figure 3**) drive the loss of ammonia during the  
 560 growing season in this part of the world.  
 561

562 An increase in ammonia concentration poses a significant and yet poorly understood effect on local and regional  
 563 air quality through the increase in PM<sub>2.5</sub> concentration. We note, however, that ammonia columns in the soil are  
 564 governed by a threshold. Higher temperatures will increase the rate of volatilization of ammonia from the soil, but  
 565 only up to a certain point where no dissolved ammonium is left. Plants, however, can also be a source of ammonia  
 566 when exposed to stressful conditions. For example, under heat stress and in instances where there **are-is** no  
 567 ammonia in the air, increase in air temperature results in exponential increase in ammonia emission from plants’  
 568 leaves (Husted and Schjoerring, 1996).

**Mis en forme :** Police : (Par défaut) +Titres CS (Times New Roman), Police de script complexe : +Titres CS (Times New Roman), 10 pt

**Mis en forme :** Police : (Par défaut) +Titres CS (Times New Roman), Police de script complexe : +Titres CS (Times New Roman), 10 pt

**Mis en forme :** Police : (Par défaut) +Titres CS (Times New Roman), Police de script complexe : +Titres CS (Times New Roman), 10 pt

**Mis en forme :** Police : (Par défaut) +Titres CS (Times New Roman), Police de script complexe : +Titres CS (Times New Roman), 10 pt

**Mis en forme :** Police : (Par défaut) +Titres CS (Times New Roman), Police de script complexe : +Titres CS (Times New Roman), 10 pt

**Mis en forme :** Police : (Par défaut) +Titres CS (Times New Roman), Police de script complexe : +Titres CS (Times New Roman), 10 pt

**Mis en forme :** Police : (Par défaut) +Titres CS (Times New Roman), Police de script complexe : +Titres CS (Times New Roman), 10 pt

**Mis en forme :** Police : (Par défaut) +Titres CS (Times New Roman), Police de script complexe : +Titres CS (Times New Roman), 10 pt



#### 5.4. Discussion and eConclusions

Agriculture worldwide has fed the human race for thousands of years, and will continue to do so, as mankind highly relies on it. Emissions from agricultural activities will inevitably increase, in order to meet the expected yield. In this study, we use a variety of state-of-the-art datasets (satellite, reanalysis and model simulation) to calculate the first regional map of ammonia emission potential during the start of the growing season in Europe. The emission potential can be used as a proxy to calculate ammonia columns in the atmosphere, and as such to assess its deposition, atmospheric transport, and contribution to PM formation. First, we show that the GEOS-Chem chemistry transport model is able to reproduce key spatio-temporal patterns of ammonia levels over Europe. The ammonia budget is governed by the emissions over source regions (North European Plain, Brittany and the Po valley), as well as by key loss processes. We find that chemical loss pathway is responsible of 50 % or more of the total ammonia loss over Europe. From the GEOS-Chem simulation, we calculate the average ammonia lifetime in the atmosphere which ranges between 4 and 12 hours in agricultural source regions of Europe. From this, and using the mass transfer coefficient for different land cover types, we calculate a range of emission potentials  $I_{soil}$  from IASI and GEOS-Chem. We find that  $I_{soil}$  ranges between from  $0.2 \times 10^{42}$  to  $9.52.5 \times 10^4$  in fertilized lands (croplands). Choosing a variable  $k$  from the literature, and based on different land cover types from MODIS, we calculate  $I_{soil}$  values that are consistent with those found in the literature. The increase in T skin is expected to have an effect on the emission of ammonia from the soil. Using T skin from the EC-Earth climate model, we estimate ammonia columns by the end of the century [2075 – 2099], and compare it to columns of the present climate [2015 – 2039]. Our results show that ammonia columns ~~might~~ will double under the SSP5-8.5 scenario, and ~~will~~ ~~might~~ increase by up to 50 % under the most likely SSP2-4.5 scenario. The eastern part of Europe is the most affected by the change in temperatures, and it is where we find the highest ammonia columns increase. Among the regions of focus, Italy, Spain, Belgium and the Netherlands are the most affected, as compared to France, England and Ireland. The highest increase in ammonia columns is observed in the Po Valley in Italy (+59 % under the SSP5-8.5).

We calculate ammonia concentration under future climate and during the start of the growing season (March) in Europe. However, in order to grasp the yearly budget of ammonia, it is crucial to apply this method to all seasons of the year; especially in regions with extensive agricultural activities, such as the United States, India, and China. In addition to this, more field measurements of ammonia emission potential ( $I_{soil}$ ) in different land use / cover types are required, this can help us perform better comparison with emission potentials calculated from model and satellite data. Finally, having ammonia columns at different times of the day, from field observations or satellite measurements will allow quantification of daily emission potentials, that will in turn help us understand its diurnal variability. This will be ensured with the launch of the Infrared Sounder (IRS) on the Meteosat Third Generation (MTG) geostationary satellites scheduled in 2025.

605  
606

## A. Appendix A

607

### 1. Ammonia-Ammonium equilibrium

608 Ammonia ( $\text{NH}_3$ ) is a water-soluble gas, it undergoes protonation with  $\text{H}^+$  from the hydronium ion  $\text{H}_3\text{O}^+$  in an  
609 aqueous solution in order to give ammonium ( $\text{NH}_4^+$  cation), the dissociation equation is expressed as follows:



610  
611

Or



612  
613

With  $K_{\text{NH}_4^+}$  as the ammonium-ammonia dissociation equilibrium constant that can be expressed as:

$$K_{\text{NH}_4^+} = \frac{[\text{NH}_3(\text{aq})][\text{H}^+]}{[\text{NH}_4^+(\text{aq})]} \quad (\text{A-3})$$

614  
615  
616  
617

The solubility of ammonia in water is affected by the temperature and the acidity (pH) of the solvent (water). The equilibrium constant can be expressed as follows:

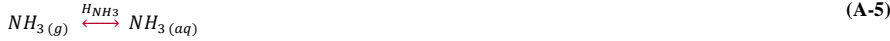
$$K_{\text{NH}_4^+} = 5.67 \cdot 10^{-10} \exp \left[ -6286 \left( \frac{1}{T} - \frac{1}{298.15} \right) \right] \quad (\text{A-4})$$

618

619

### 2. Henry's equilibrium

620 Upon its dissolution in water,  $\text{NH}_3$  obeys the Henry's law. Ammonia gas ( $\text{NH}_3(\text{g})$ ) near the surface of the solvent  
621 is in equilibrium with the dissolved ammonia in the aqueous phase  $\text{NH}_3(\text{aq})$  (in water). Henry's equilibrium is  
622 expressed as follows:



623  
624

With where  $H_{\text{NH}_3}$  as the Henry's constant, which it can be expressed as follows (Wichink Kruit, 2010):

$$H_{\text{NH}_3} = \frac{[\text{NH}_3(\text{aq})]}{[\text{NH}_3(\text{g})]} = 5.527 \cdot 10^{-4} \cdot \exp \left[ 4092 \left( \frac{1}{T} - \frac{1}{298.15} \right) \right] \quad (\text{A-6})$$

625  
626  
627

The partial pressure of ammonia near the surface of the soil can be calculated using Henry's constant and the dissociation equilibrium (Wichink Kruit, 2010):

$$P_{\text{NH}_3} = \frac{K_{\text{NH}_4^+} [\text{NH}_4^+]}{H_{\text{NH}_3} [\text{H}^+]} = \frac{5.67 \cdot 10^{-10} \cdot \exp \left[ -6286 \left( \frac{1}{T} - \frac{1}{298.15} \right) \right]}{5.527 \cdot 10^{-4} \cdot \exp \left[ 4092 \left( \frac{1}{T} - \frac{1}{298.15} \right) \right]} \times \frac{[\text{NH}_4^+]}{[\text{H}^+]} \quad (\text{A-7})$$

628  
629  
630

If we use the ideal gas law ( $PV=nRT$ ), we can draw the link between the mass density of ammonia ( $\text{NH}_3(\text{g})$ ) and the partial pressure:

$$\chi_{\text{NH}_3} = \frac{P_{\text{NH}_3} \cdot M_{\text{NH}_3}}{R \cdot T} \quad (\text{A-8})$$

631  
632  
633  
634

Where  $\chi_{\text{NH}_3}$  is the concentration of  $\text{NH}_3$  at the soil surface ( $\text{kg m}^{-3}$ ),  $P_{\text{NH}_3}$  is the partial pressure of  $\text{NH}_3$  near the surface (atm),  $M_{\text{NH}_3}$  is the molar mass of  $\text{NH}_3$  ( $\text{kg mol}^{-1}$ ),  $R$  is the gas constant ( $0.082 \text{ atm L mol}^{-1} \text{ K}^{-1}$ ), and  $T$  is the temperature in Kelvin.

635

Substituting Eq. (A-7) (A-5) into (A-8)(A-6) we get:

$$\chi_{\text{NH}_3} = \frac{2.75 \cdot 10^9 \left( \frac{\text{gK}}{\text{m}^3} \right)}{T_{\text{soil}}} \exp \left[ \frac{-1.04 \cdot 10^4}{T_{\text{soil}}} \right] \Gamma_{\text{soil}} \quad (\text{A-9})$$

636  
637  
638  
639

Where  $\chi_{\text{NH}_3}$  is the concentration of ammonia at the soil surface at equilibrium ( $\text{g m}^{-3}$ ), and is referred to as the compensation point,  $T_{\text{soil}}$  is the temperature of the soil (Kelvin),  $\Gamma_{\text{NH}_3}$  is the  $\text{NH}_3$  emission potential from the soil and is a dimensionless ratio between  $[\text{NH}_4^+]$  and  $[\text{H}^+]$ .

640 **3. Ammonia total columns from IASI**

641 In this study we use the total columns of ammonia from IASI (molecules m<sup>-2</sup>) since in order to calculate the  
 642 emission potential  $\Gamma_{soil}$ , we should draw the link between these columns and this parameter. The bi-directional  
 643 exchange of NH<sub>3</sub> between the surface and the atmosphere can be expressed by the flux (assuming a flux  
 644 independent of time) (Roelle and Aneja, 2005; Zhang et al., 2010):

$$Flux_{NH_3} = k ([NH_3]^{soil} - [NH_3]^{atm}) \quad (\text{A-10})$$

645 wWhere  $Flux_{NH_3}$  is the bidirectional flux between the soil and the atmosphere (molecules (m<sup>2</sup> s<sup>-1</sup>)),  $k$  is the soil –  
 646 atmosphere exchange velocity (m s<sup>-1</sup>), also known as the mass transfer coefficient;  $[NH_3]^{soil}$  is the concentration  
 647 of NH<sub>3(g)</sub> in the soil, and  $[NH_3]^{atm}$  is the concentration of NH<sub>3(g)</sub> in the atmosphere near the surface (molecules m<sup>-3</sup>).  
 648 We can consider that  $[NH_3]^{atm}$  is identical to the total column of NH<sub>3</sub> provided by IASI and denoted here as  
 649  $[NH_3]^{col}$ . This is because most of the atmospheric NH<sub>3</sub> are located in the lower boundary layer (Dammers et al.,  
 650 2019).

651 Assuming a first order dissociation of NH<sub>3</sub>, we can express the change in the  $[NH_3]^{col}$  total columns as follows:

$$\frac{d [NH_3]^{col}}{dt} = Flux_{NH_3} - k' [NH_3]^{col} \quad (\text{A-11})$$

653 Where  $k'$  is the rate of dissociation of first order  $k' = 1/\tau$  (m s<sup>-1</sup>), with  $\tau$  the lifetime of NH<sub>3</sub> in the atmosphere.  
 654 Assuming steady state, and considering the  $[NH_3]^{atm}$  as the  $[NH_3]^{col}$ , and  $[NH_3]^{soil}$  as  $\chi_{NH_3}$ , Eq. (A-11) (A-9)  
 655 can be written as:

$$k \left( \frac{N_a \cdot \chi_{NH_3}}{M_{NH_3}} - \frac{1}{c} [NH_3]^{col} \right) = \frac{[NH_3]^{col}}{\tau} \quad (\text{A-12})$$

657 Where  $c$  is the column height and is equal to 6 km. It is important to note that we neglect the effect of transport by  
 658 wind since we only look at large regions. Finally, the total column of ammonia  $[NH_3]^{col}$  can be written as:

$$[NH_3]^{col} = \frac{N_a \cdot \chi_{NH_3}}{M_{NH_3} \cdot (c + \frac{1}{k\tau})} \quad (\text{A-13})$$

660 The column height is not considered anymore because it is negligible compared to  $1/k\tau$ , using Eq. (A-9) (A-6)  
 661 into (A-13) (A-11) we get:

$$[NH_3]^{col} = \frac{2.75 \cdot 10^{27} \left( \frac{gK}{cm^3} \right)}{T_{soil}} \exp \left[ \frac{-1.04 \cdot 10^4}{T_{soil}} \right] \Gamma_{NH_3} \cdot k\tau \quad \left( \frac{\text{molecules}}{cm^2} \right) \quad (\text{A-14})$$

663 Note that  $2.75 \cdot 10^{27} = \frac{a \cdot N_a \cdot c'}{M_{NH_3}} \left( \frac{K \text{ molecules}}{cm^3} \right)$ , where  $a = 2.75 \cdot 10^3$  (g K cm<sup>-3</sup>),  $N_a$  Avogadro's number  
 664 (6.0221409 × 10<sup>23</sup> molecules mol<sup>-1</sup>), 10<sup>-2</sup> is added to convert  $k$  from m s<sup>-1</sup> to cm s<sup>-1</sup>, and  $M_{NH_3}$  the molar mass of  
 665 NH<sub>3</sub> (17.031 g mol<sup>-1</sup>). The emission potential of NH<sub>3</sub> from the soil can we written as:

$$\Gamma_{soil} = \frac{[NH_3]^{col} \cdot T_{soil}}{\exp \left( \frac{-b}{T_{soil}} \right)} \frac{M_{NH_3}}{a \cdot N_a \cdot 10^{-2} \cdot k\tau} \quad (\text{A-15})$$

667 wWhere  $b = 1.04 \times 10^4$  K.  
 668

Mis en forme : Indice

Mis en forme : Indice

### Author contribution

670 RA contributed to the conception and design of the article, developed the code, wrote the manuscript, analysed and  
interpreted of the data, and approved the version for submission; CV, CC, and PFC revised the manuscript; WCP provided  
the GEOS-Chem simulation data, and revised the manuscript; NE provided ammonia lifetime calculation using the LMDz-  
OR-INCA chemistry transport model and commented on the manuscript; MVD and LC contributed to the acquisition of the  
IASI ammonia data (NH<sub>3</sub>-v3R-ERA5), and revised the manuscript; SS contributed to the conception and design of the article,  
675 provided the EC-Earth temperature data, and revised the manuscript, and approved the version for submission.

### Acknowledgments

The IASI mission is a joint mission of Eumetsat and the Centre National d'Etudes Spatiales (CNES, France). The authors  
acknowledge the Aeris data infrastructure for providing the IASI L1C and L2 data.

### Funding information

680 Rimal Abeer is grateful to CNES for financial support. The research in Belgium was funded by the Belgian State Federal  
Office for Scientific, Technical and Cultural Affairs (Prodex HIRS) and the Air Liquide Foundation (TAPIR project). This  
work is also partly supported by the FED-iWIN project ARENBERG ("Assessing the Reactive Nitrogen Budget and Emissions  
at Regional and Global Scales") funded via the Belgian Science Policy Office (BELSPO). L. Clarisse is Research Associate  
supported by the Belgian F.R.S.-FNRS. C. Clerboux is grateful to CNES for scientific collaboration and financial support. N.  
685 Evangeliou was funded by Norges Forskningsråd (ROM- FORSK – Program for romforskning of the Research Council of  
Norway (grant no. 275407)).

### Competing interests

The authors are aware of no competing interests.

### Data accessibility statement

690 The IASI-NH<sub>3</sub> used in this study are retrieved from the Aeris data infrastructure (<https://iasi.aeris-data.fr/nh3r-era5/>). ERA5  
skin temperature from 1979 to present are available for download in the following DOI: [10.24381/cds.adbb2d47](https://doi.org/10.24381/cds.adbb2d47). The GEOS-  
Chem outputs used in this study are only available upon request. EC-Earth3 model output prepared for CMIP6 ScenarioMIP  
are retrieved here: <https://doi.org/10.22033/ESGF/CMIP6.727>. The MODIS land cover data are available for download in the  
following link: <https://doi.org/10.5067/MODIS/MCD12Q1.006>.  
695

700

## References

- Abeed, R., Clerbaux, C., Clarisse, L., Van Damme, M., Coheur, P.-F., and Safieddine, S. A space view of agricultural and industrial changes during the Syrian civil war. *Elem. Sci. Anthr.* <https://doi.org/10.1525/elementa.2021.000041> (2021)
- 710 Adams, C., McLinden, C. A., Shephard, M. W., Dickson, N., Dammers, E., Chen, J., Makar, P., Cady-Pereira, K. E., Tam, N., Kharol, S. K., Lamsal, L. N., and Krotkov, N. A. Satellite-derived emissions of carbon monoxide, ammonia, and nitrogen dioxide from the 2016 Horse River wildfire in the Fort McMurray area. *Atmospheric Chem. Phys.* <https://doi.org/10.5194/acp-19-2577-2019> (2019)
- 715 Agreste. (2014). *Enquête Pratiques culturales 2011—Grandes cultures et prairies / Agreste, la statistique agricole (No. 21; Agreste Les Dossiers)*. Ministère de l'Agriculture, de l'Agroalimentaire et de la Forêt. <https://agreste.agriculture.gouv.fr/agreste-web/disaron/dos21/detail/>.
- Alexander, B., Sherwen, T., Holmes, C. D., Fisher, J. A., Chen, Q., Evans, M. J., and Kasibhatla, P. Global inorganic nitrate production mechanisms: Comparison of a global model with nitrate isotope observations. *Atmospheric Chem. Phys.* <https://doi.org/10.5194/acp-20-3859-2020> (2020)
- 720 Aneja, V. P., Rogers, H. H., and Stahel, E. P. Dry Deposition of Ammonia at Environmental Concentrations on Selected Plant Species. *J. Air Pollut. Control Assoc.* <https://doi.org/10.1080/00022470.1986.10466183> (1986)
- AQEG. *Fine particulate matter (PM2.5) in the United Kingdom* (p. 203). Air Quality Expert Group (AQEG), prepared for the Department for Environment, Food and Rural Affairs (Defra), Scottish Executive, Welsh Government and the Department of the Environment in Northern Ireland. [https://uk-air.defra.gov.uk/assets/documents/reports/cat11/1212141150\\_AQEG\\_Fine\\_Partuculate\\_Matter\\_in\\_the\\_UK.pdf](https://uk-air.defra.gov.uk/assets/documents/reports/cat11/1212141150_AQEG_Fine_Partuculate_Matter_in_the_UK.pdf)
- 725 (2012)
- Barnes, A. P., Svensson, C., and Kjeldsen, T. R. North Atlantic air pressure and temperature conditions associated with heavy rainfall in Great Britain. *Int. J. Climatol.* <https://doi.org/10.1002/joc.7414> (2022)
- Bauer, S. E., Tsigaridis, K., and Miller, R. Significant atmospheric aerosol pollution caused by world food cultivation. *Geophys. Res. Lett.* <https://doi.org/10.1002/2016GL068354> (2016)
- 730 Behera, S. N., Sharma, M., Aneja, V. P., and Balasubramanian, R. Ammonia in the atmosphere: A review on emission sources, atmospheric chemistry and deposition on terrestrial bodies. *Env. Sci Pollut Res.* <https://doi.org/10.1007/s11356-013-2051-9> (2013)
- 735 Belward, A. S., Estes, John E., and Kline, K. D. The IGBP-DIS Global 1-Km Land-Cover Data Set DIS-Cover: A Project Overview. *Photogramm. Eng. Remote Sens.* [https://www.asprs.org/wp-content/uploads/pers/1999journal/sep/1999\\_sept\\_1013-1020.pdf](https://www.asprs.org/wp-content/uploads/pers/1999journal/sep/1999_sept_1013-1020.pdf) (1999)
- Bey, I., Jacob, D. J., Yantosca, R. M., Logan, J. A., Field, B. D., Fiore, A. M., Li, Q., Liu, H. Y., Mickley, L. J., and Schultz, M. G. Global modeling of tropospheric chemistry with assimilated meteorology: Model description and evaluation. *J. Geophys. Res. Atmospheres.* <https://doi.org/10.1029/2001JD000807> (2001)
- 740 Bouwman, A. F., Lee, D. S., Asman, W. a. H., Dentener, F. J., Van Der Hoek, K. W., and Olivier, J. G. J. A global high-resolution emission inventory for ammonia. *Glob. Biogeochem. Cycles.* <https://doi.org/10.1029/97GB02266> (1997)
- Clarisse, L., Van Damme, M., Clerbaux, C., and Coheur, P.-F. Tracking down global NH<sub>3</sub> point sources with wind-adjusted superresolution. *Atmospheric Meas. Tech.* <https://doi.org/10.5194/amt-12-5457-2019> (2019)
- 745 Clarisse, L., Van Damme, M., Gardner, W., Coheur, P.-F., Clerbaux, C., Whitburn, S., Hadji-Lazaro, J., and Hurtmans, D. Atmospheric ammonia (NH<sub>3</sub>) emanations from Lake Natron's saline mudflats. *Sci. Rep.* <https://doi.org/10.1038/s41598-019-39935-3> (2019)
- Clerbaux, C., Boynard, A., Clarisse, L., George, M., Hadji-Lazaro, J., Herbin, H., Hurtmans, D., Pommier, M., Razavi, A., Turquety, S., and Wespes, C. Monitoring of atmospheric composition using the thermal infrared IASI/MetOp sounder. *Atmospheric Chem. Phys.* <https://doi.org/10.5194/acp-9-6041-2009> (2009)

Mis en forme : Justifié

Mis en forme : Français (France)

Mis en forme : Français (France)

Mis en forme : Français (France)

Code de champ modifié

Mis en forme : Police : (Par défaut) +Titres (Times New Roman), 10 pt, Police de script complexe :+Titres (Times New Roman), 10 pt

Mis en forme : Justifié

Mis en forme : Police : (Par défaut) +Titres (Times New Roman), 10 pt, Police de script complexe :+Titres (Times New Roman), 10 pt

Mis en forme : Police : (Par défaut) +Titres (Times New Roman), 10 pt, Police de script complexe :+Titres (Times New Roman), 10 pt

Mis en forme : Français (France)

750 Coheur, P.-F., Clarisse, L., Turquety, S., Hurtmans, D., and Clerbaux, C. IASI measurements of reactive trace species in biomass burning plumes. *Atmospheric Chem. Phys.* <https://doi.org/10.5194/acp-9-5655-2009> (2009)

Dammers, E., McLinden, C. A., Griffin, D., Shephard, M. W., Van Der Graaf, S., Lutsch, E., Schaap, M., Gainairu-Matz, Y., Fioletov, V., Van Damme, M., Whitburn, S., Clarisse, L., Cady-Pereira, K., Clerbaux, C., Coheur, P. F., and Erismann, J. W. NH<sub>3</sub> emissions from large point sources derived from CrIS and IASI satellite observations. *Atmospheric Chem. Phys.* <https://doi.org/10.5194/acp-19-12261-2019> (2019)

755 David, M., Loubet, B., Cellier, P., Mattsson, M., Schjoerring, J. K., Nemitz, E., Roche, R., Riedo, M., and Sutton, M. A. Ammonia sources and sinks in an intensively managed grassland canopy. *Biogeosciences.* <https://doi.org/10.5194/bg-6-1903-2009> (2009)

760 Donnelly, C., Greuell, W., Andersson, J., Gerten, D., Pisacane, G., Roudier, P., and Ludwig, F. Impacts of climate change on European hydrology at 1.5, 2 and 3 degrees mean global warming above preindustrial level. *Clim. Change.* <https://doi.org/10.1007/s10584-017-1971-7> (2017)

Döscher, R., Acosta, M., Alessandri, A., Anthoni, P., Armeth, A., Arsouze, T., Bergmann, T., Bernadello, R., Boussetta, S., Caron, L.-P., Carver, G., Castrillo, M., Catalano, F., Cvijanovic, I., Davini, P., Dekker, E., Doblas-Reyes, F. J., Docquier, D., Echevarria, P., ... Zhang, Q. The EC-Earth3 Earth System Model for the Climate Model Intercomparison Project 6. *Geosci. Model Dev. Discuss.* <https://doi.org/10.5194/gmd-2020-446> (2021)

765 ECMWF. *IFS Documentation CY43R1*. ECMWF. <https://www.ecmwf.int/sites/default/files/elibrary/2016/17117-part-iv-physical-processes.pdf> (2016)

EDO, G. D. O. *Drought news in Europe: Situation in April 2011—Short Analysis of data from the European Drought Observatory (EDO)* (p. 2). <https://edo.jrc.ec.europa.eu/documents/news/EDODroughtNews201104.pdf> (2011)

770 [Einarsson, R., Sanz-Cobena, A., Aguilera, E., Billen, G., Garnier, J., van Grinsven, H. J. M., & Lassaletta, L. \(2021\). Crop production and nitrogen use in European cropland and grassland 1961–2019. \*Scientific Data\*, 8\(1\), Article 1. <https://doi.org/10.1038/s41597-021-01061-z>](https://doi.org/10.1038/s41597-021-01061-z)

Erismann, J. W., Van Pul, A., and Wyers, P. Parametrization of surface resistance for the quantification of atmospheric deposition of acidifying pollutants and ozone. *Atmos. Environ.* [https://doi.org/10.1016/1352-2310\(94\)90433-2](https://doi.org/10.1016/1352-2310(94)90433-2) (1994)

775 [European Environment Agency. \*Nitrogen Dioxide \(NO<sub>2</sub>\): annual mean concentrations in Europe.\* <https://www.eea.europa.eu/themes/air/interactive/no2> \(2017a\)](https://www.eea.europa.eu/themes/air/interactive/no2)

[European Environment Agency. \*Sulphur Dioxide \(SO<sub>2</sub>\): annual mean concentrations in Europe.\* <https://www.eea.europa.eu/themes/air/interactive/so2> \(2017b\)](https://www.eea.europa.eu/themes/air/interactive/so2)

780 [European Environment Agency. \*Global and European temperatures.\* <https://www.eea.europa.eu/ims/global-and-european-temperatures> \(2022\)](https://www.eea.europa.eu/ims/global-and-european-temperatures)

Evangeliou, N., Balkanski, Y., Eckhardt, S., Cozic, A., Van Damme, M., Coheur, P.-F., Clarisse, L., Shephard, M., Cady-Pereira, K., and Hauglustaine, D. 10-year satellite-constrained fluxes of ammonia improve performance of chemistry transport models. *Atmospheric Chem. Phys.* <https://doi.org/10.5194/acp-21-4431-2021> (2021)

785 Eyering, V., Bony, S., Meehl, G. A., Senior, C. A., Stevens, B., Stouffer, R. J., and Taylor, K. E. Overview of the Coupled Model Intercomparison Project Phase 6 (CMIP6) experimental design and organization. *Geosci. Model Dev.* <https://doi.org/10.5194/gmd-9-1937-2016> (2016)

FAO. *FAO, GIEWS, Earth Observation.* <https://www.fao.org/giews/earthobservation/country/index.jsp?lang=en&ancode=FRA> (2022)

790 [Fertilizers Europe. \*Infinite Fertilizers—Nutrient Stewardship.\* <https://www.fertilizerseurope.com/wp-content/uploads/2019/08/Nutrient-Stewardship-Sept-2016-website.pdf>. \(2016\)](https://www.fertilizerseurope.com/wp-content/uploads/2019/08/Nutrient-Stewardship-Sept-2016-website.pdf)

Flechard, C. R., Massad, R.-S., Loubet, B., Personne, E., Simpson, D., Bash, J. O., Cooter, E. J., Nemitz, E., and Sutton, M. A. Advances in understanding, models and parameterizations of biosphere-atmosphere ammonia exchange. *Biogeosciences.* <https://doi.org/10.5194/bg-10-5183-2013> (2013)

795 Flechard, C. R., Nemitz, E., Smith, R. I., Fowler, D., Vermeulen, A. T., Bleeker, A., Erismann, J. W., Simpson, D., Zhang, L., Tang, Y. S., and Sutton, M. A. Dry deposition of reactive nitrogen to European ecosystems: A comparison of inferential models across the NitroEurope network. *Atmospheric Chem. Phys.* <https://doi.org/10.5194/acp-11-2703-2011> (2011)

**Code de champ modifié**

**Mis en forme :** Police :(Par défaut) +Titres (Times New Roman), 10 pt, Police de script complexe :+Titres (Times New Roman), 10 pt

**Mis en forme :** Justifié

**Mis en forme :** Police :(Par défaut) +Titres (Times New Roman), 10 pt, Police de script complexe :+Titres (Times New Roman)

**Mis en forme :** Police :(Par défaut) +Titres (Times New Roman), Police de script complexe :+Titres (Times New Roman)

**Mis en forme :** Police :Italique, Police de script complexe :Italique

**Mis en forme :** Police :Italique, Police de script complexe :Italique, Indice

**Mis en forme :** Police :Italique, Police de script complexe :Italique

**Code de champ modifié**

**Mis en forme :** Police :Italique, Police de script complexe :Italique

**Mis en forme :** Police :Italique, Police de script complexe :Italique, Indice

**Mis en forme :** Police :Italique, Police de script complexe :Italique

**Mis en forme :** Police :10 pt

**Mis en forme :** Police :10 pt, Police de script complexe :10 pt

**Mis en forme :** Police :10 pt, Police de script complexe :10 pt

**Mis en forme :** Police :10 pt, Couleur de police : Automatique, Police de script complexe :10 pt

**Mis en forme :** Police :(Par défaut) +Titres (Times New Roman), 10 pt, Police de script complexe :+Titres (Times New Roman), 10 pt

**Mis en forme :** Justifié

**Code de champ modifié**

**Mis en forme :** Lien hypertexte, Police :(Par défaut) +Titres (Times New Roman), 10 pt, Police de script complexe :+Titres (Times New Roman), 10 pt

- Flechard, C. R., Spirig, C., Neftel, A., and Ammann, C. The annual ammonia budget of fertilised cut grassland – Part 2: Seasonal variations and compensation point modeling. *Biogeosciences*. <https://doi.org/10.5194/bg-7-537-2010> (2010)
- 800 Folberth, G. A., Hauglustaine, D. A., Lathière, J., and Brocheton, F. Interactive chemistry in the Laboratoire de Météorologie Dynamique general circulation model: Model description and impact analysis of biogenic hydrocarbons on tropospheric chemistry. *Atmospheric Chem. Phys.* <https://doi.org/10.5194/acp-6-2273-2006> (2006)
- Garrido-Perez, J. M., Ordóñez, C., García-Herrera, R., and Barriopedro, D. Air stagnation in Europe: Spatiotemporal variability and impact on air quality. *Sci. Total Environ.* <https://doi.org/10.1016/j.scitotenv.2018.07.238> (2018)
- 805 Gelaro, R., McCarty, W., Suárez, M. J., Todling, R., Molod, A., Takacs, L., Randles, C. A., Darmenov, A., Bosilovich, M. G., Reichle, R., Wargan, K., Coy, L., Cullather, R., Draper, C., Akella, S., Buchard, V., Conaty, A., Silva, A. M. da, Gu, W., ... Zhao, B. The Modern-Era Retrospective Analysis for Research and Applications, Version 2 (MERRA-2). *J. Clim.* <https://doi.org/10.1175/JCLI-D-16-0758.1> (2017)
- 810 Hersbach, H., Bell, B., Berrisford, P., Hirahara, S., Horányi, A., Muñoz-Sabater, J., Nicolas, J., Peubey, C., Radu, R., Schepers, D., Simmons, A., Soci, C., Abdalla, S., Abellan, X., Balsamo, G., Bechtold, P., Biavati, G., Bidlot, J., Bonavita, M., ... Thépaut, J.-N. The ERA5 global reanalysis. *Q. J. R. Meteorol. Soc.* <https://doi.org/10.1002/qj.3803> (2020)
- Hoesly, R. M., Smith, S. J., Feng, L., Klimont, Z., Janssens-Maenhout, G., Pitkanen, T., Seibert, J. J., Vu, L., Andres, R. J., Bolt, R. M., Bond, T. C., Dawidowski, L., Kholod, N., Kurokawa, J., Li, M., Liu, L., Lu, Z., Moura, M. C. P., O'Rourke, P. R., and Zhang, Q. Historical (1750–2014) anthropogenic emissions of reactive gases and aerosols from the Community Emissions Data System (CEDS). *Geosci. Model Dev.* <https://doi.org/10.5194/gmd-11-369-2018> (2018)
- 815 Hourdin, F., Musat, I., Bony, S., Braconnot, P., Codron, F., Dufresne, J.-L., Fairhead, L., Filiberti, M.-A., Friedlingstein, P., Grandpeix, J.-Y., Krinner, G., LeVan, P., Li, Z.-X., and Lott, F. The LMDZ4 general circulation model: Climate performance and sensitivity to parametrized physics with emphasis on tropical convection. *Clim. Dyn.* <https://doi.org/10.1007/s00382-006-0158-0> (2006)
- 820 Husted, S., and Schjoerring, J. K. Ammonia Flux between Oilseed Rape Plants and the Atmosphere in Response to Changes in Leaf Temperature, Light Intensity, and Air Humidity (Interactions with Leaf Conductance and Apoplastic NH<sub>4</sub><sup>+</sup> and H<sup>+</sup> Concentrations). *Plant Physiol.* <https://doi.org/10.1104/pp.112.1.67> (1996)
- 825 Jacob, D., Kotova, L., Teichmann, C., Sobolowski, S. P., Vautard, R., Donnelly, C., Koutroulis, A. G., Grillakis, M. G., Tsanis, I. K., Damm, A., Sakallii, A., and van Vliet, M. T. H. Climate Impacts in Europe Under +1.5°C Global Warming. *Earths Future*. <https://doi.org/10.1002/2017EF000710> (2018)
- Keller, C. A., Long, M. S., Yantosca, R. M., Da Silva, A. M., Pawson, S., and Jacob, D. J. HEMCO v1.0: A versatile, ESMF-compliant component for calculating emissions in atmospheric models. *Geosci. Model Dev.* <https://doi.org/10.5194/gmd-7-1409-2014> (2014)
- 830 Klaes, K. D. The EUMETSAT Polar System. *Comprehensive Remote Sensing*. Elsevier. <https://doi.org/10.1016/B978-0-12-409548-9.10318-5> (2018)
- Krinner, G., Viovy, N., de Noblet-Ducoudré, N., Ogée, J., Polcher, J., Friedlingstein, P., Ciais, P., Sitch, S., and Prentice, I. C. A dynamic global vegetation model for studies of the coupled atmosphere-biosphere system. *Glob. Biogeochem. Cycles*. <https://doi.org/10.1029/2003GB002199> (2005)
- 835 Lee, W., An, S., and Choi, Y. Ammonia harvesting via membrane gas extraction at moderately alkaline pH: A step toward net-profitable nitrogen recovery from domestic wastewater. *Chem. Eng. J.* <https://doi.org/10.1016/j.cej.2020.126662> (2020)
- Lentze, G. *Metop-A satellite retiring after 15 years of huge benefits to forecasting* [Text]. ECMWF. ECMWF. <https://www.ecmwf.int/en/about/media-centre/news/2021/metop-satellite-retiring-after-15-years-huge-benefits-forecasting> (2021, November 12)
- 840 Luo, Z., Zhang, Y., Chen, W., Van Damme, M., Coheur, P.-F., and Clarisse, L. Estimating global ammonia (NH<sub>3</sub>) emissions based on IASI observations from 2008 to 2018. *Atmospheric Chem. Phys.* <https://doi.org/10.5194/acp-22-10375-2022> (2022)
- 845 Massad, R.-S., Nemitz, E., and Sutton, M. A. Review and parameterisation of bi-directional ammonia exchange between vegetation and the atmosphere. *Atmospheric Chem. Phys.* <https://doi.org/10.5194/acp-10-10359-2010> (2010)

- Masson-Delmotte, V., P. Zhai, A. Pirani, S.L., Connors, C. Péan, S. Berger, N. Caud, Y. Chen, L. Goldfarb, M.I. Gomis, M. Huang, K. Leitzell, E. Lonnoy, J.B.R., and Matthews, T.K. Maycock, T. Waterfield, O. Yelekçi, R. Yu, and B. Zhou. *IPCC, 2021: Climate Change 2021: The Physical Science Basis. Contribution of Working Group I to the Sixth Assessment Report of the Intergovernmental Panel on Climate Change*. Cambridge University Press. In Press. <https://www.ipcc.ch/assessment-report/ar6/> (2021)
- Mattsson, M., B. H., M. D., Loubet, B., M. R., Theobald, M., Sutton, M., Bruhn, D., Neftel, A., and Schjoerring, J. Temporal variability in bioassays of ammonia emission potential in relation to plant and soil N parameters in intensively managed grassland. *Biogeosciences Discuss.* <https://doi.org/10.5194/bgd-5-2749-2008> (2008)
- 855 McDuffie, E. E., Smith, S. J., O'Rourke, P., Tibrewal, K., Venkataraman, C., Marais, E. A., Zheng, B., Crippa, M., Brauer, M., and Martin, R. V. A global anthropogenic emission inventory of atmospheric pollutants from sector- and fuel-specific sources (1970–2017): An application of the Community Emissions Data System (CEDS). *Earth Syst. Sci. Data.* <https://doi.org/10.5194/essd-12-3413-2020> (2020)
- 860 Met Office. *Exceptionally warm and dry Spring 2011*. Met Office. <https://www.metoffice.gov.uk/binaries/content/assets/metofficegovuk/pdf/weather/learn-about/uk-past-events/interesting/2011/exceptionally-warm-and-dry-spring-2011---met-office.pdf> (2016)
- Nemitz, E., Sutton, M. A., Schjoerring, J. K., Husted, S., and Paul Wyers, G. Resistance modelling of ammonia exchange over oilseed rape. *Agric. For. Meteorol.* [https://doi.org/10.1016/S0168-1923\(00\)00206-9](https://doi.org/10.1016/S0168-1923(00)00206-9) (2000)
- Olesen, J. E., and Sommer, S. G. Modelling effects of wind speed and surface cover on ammonia volatilization from stored pig slurry. *Atmospheric Environ. Part Gen. Top.* [https://doi.org/10.1016/0960-1686\(93\)90030-3](https://doi.org/10.1016/0960-1686(93)90030-3) (1993)
- 865 Personne, E., Tardy, F., Générumont, S., Decuq, C., Gueudet, J.-C., Mascher, N., Durand, B., Masson, S., Lauransot, M., Fléchar, C., Burkhardt, J., and Loubet, B. Investigating sources and sinks for ammonia exchanges between the atmosphere and a wheat canopy following slurry application with trailing hose. *Agric. For. Meteorol.* <https://doi.org/10.1016/j.agrformet.2015.03.002> (2015)
- 870 Phillips, S. B., Arya, S. P., and Aneja, V. P. Ammonia flux and dry deposition velocity from near-surface concentration gradient measurements over a grass surface in North Carolina. *Atmos. Environ.* <https://doi.org/10.1016/j.atmosenv.2004.02.054> (2004)
- Pinder, R. W., Gilliland, A. B., and Dennis, R. L. Environmental impact of atmospheric NH<sub>3</sub> emissions under present and future conditions in the eastern United States. *Geophys. Res. Lett.* <https://doi.org/10.1029/2008GL033732> (2008)
- 875 Plumb, R. A., and Stolarski, R. S. Chapter 2: The Theory of Estimating Lifetimes Using Models and Observations. *SPARC Lifetimes Rep. 2013 – SPARC Rep. No 6.* [https://pages.jh.edu/rstolar/other\\_pubs/LifetimeReport\\_Ch2.pdf](https://pages.jh.edu/rstolar/other_pubs/LifetimeReport_Ch2.pdf) (2013)
- Potapov, P., Turubanova, S., Hansen, M. C., Tyukavina, A., Zalles, V., Khan, A., Song, X.-P., Pickens, A., Shen, Q., and Cortez, J. Global maps of cropland extent and change show accelerated cropland expansion in the twenty-first century. *Nat. Food.* <https://doi.org/10.1038/s43016-021-00429-z> (2022)
- 880 Randerson, J. T., Van Der Werf, G. R., Giglio, L., Collatz, G. J., and Kasibhatla, P. S. Global Fire Emissions Database, Version 4.1 (GFEDv4). *ORNL DAAC.* <https://doi.org/10.3334/ORNLDAAC/1293> (2015)
- Riahi, K., van Vuuren, D. P., Kriegler, E., Edmonds, J., O'Neill, B. C., Fujimori, S., Bauer, N., Calvin, K., Dellink, R., Fricko, O., Lutz, W., Popp, A., Cuaresma, J. C., Ke, S., Leimbach, M., Jiang, L., Kram, T., Rao, S., Emmerling, J., ... Tavoni, M. The Shared Socioeconomic Pathways and their energy, land use, and greenhouse gas emissions implications: An overview. *Glob. Environ. Change.* <https://doi.org/10.1016/j.gloenvcha.2016.05.009> (2017)
- 885 Roelle, P. A., and Aneja, V. P. Modeling of Ammonia Emissions from Soils. *Environ. Eng. Sci.* <https://doi.org/10.1089/ees.2005.22.58> (2005)
- Schlesinger, W. H., and Hartley, A. E. A global budget for atmospheric NH<sub>3</sub>. *Biogeochemistry.* <https://doi.org/10.1007/BF00002936> (1992)
- 890 Shen, H., Chen, Y., Hu, Y., Ran, L., Lam, S. K., Pavur, G. K., Zhou, F., Pleim, J. E., and Russell, A. G. Intense Warming Will Significantly Increase Cropland Ammonia Volatilization Threatening Food Security and Ecosystem Health. *One Earth.* <https://doi.org/10.1016/j.oneear.2020.06.015> (2020)
- Shephard, M. W., and Cady-Pereira, K. E. Cross-track Infrared Sounder (CrIS) satellite observations of tropospheric ammonia. *Atmos Meas Tech.* <https://doi.org/10.5194/amt-8-1323-2015> (2015)
- 895 Sulla-Menashe, D., and Friedl, M. A. *User Guide to Collection 6 MODIS Land Cover (MCD12Q1 and MCD12C1) Product.* [https://lpdaac.usgs.gov/documents/101/MCD12\\_User\\_Guide\\_V6.pdf](https://lpdaac.usgs.gov/documents/101/MCD12_User_Guide_V6.pdf) (2018)



- Svensson, L., and Ferm, M. Mass Transfer Coefficient and Equilibrium Concentration as Key Factors in a New Approach to Estimate Ammonia Emission from Livestock Manure. *J. Agric. Eng. Res.* <https://doi.org/10.1006/jaer.1993.1056> (1993)
- 900 Theobald, M. R., Crittenden, P. D., Hunt, A. P., Tang, Y. S., Dragosits, U., and Sutton, M. A. Ammonia emissions from a Cape fur seal colony, Cape Cross, Namibia. *Geophys. Res. Lett.* <https://doi.org/10.1029/2005GL024384> (2006)
- Tournadre, B., Chelin, P., Ray, M., Cuesta, J., Kutzner, R. D., Landsheere, X., Fortems-Cheiney, A., Flaud, J.-M., Hase, F., Blumenstock, T., Orphal, J., Viatte, C., and Camy-Peyret, C. Atmospheric ammonia (NH<sub>3</sub>) over the Paris megacity: 9 years of total column observations from ground-based infrared remote sensing. *Atmospheric Meas. Tech.* <https://doi.org/10.5194/amt-13-3923-2020> (2020)
- 905 USDA. *Europe—Crop Calendars*. Foreign Agric. Serv. US Dep. Agric. Foreign Agricultural Service, U.S. Department of Agriculture. [https://ipad.fas.usda.gov/rssiws/al/crop\\_calendar/europe.aspx](https://ipad.fas.usda.gov/rssiws/al/crop_calendar/europe.aspx) (2022, May 12)
- Van Damme, M., Clarisse, L., Franco, B., Sutton, M. A., Erisman, J. W., Wichink Kruit, R., van Zanten, M., Whitburn, S., Hadji-Lazaro, J., Hurtmans, D., Clerbaux, C., and Coheur, P.-F. Global, regional and national trends of atmospheric ammonia derived from a decadal (2008–2018) satellite record. *Environ. Res. Lett.* <https://doi.org/10.1088/1748-9326/abd5e0> (2021)
- Van Damme, M., Clarisse, L., Whitburn, S., Hadji-Lazaro, J., Hurtmans, D., Clerbaux, C., and Coheur, P.-F. Industrial and agricultural ammonia point sources exposed. *Nature*. <https://doi.org/10.1038/s41586-018-0747-1> (2018)
- Van Damme, M., Whitburn, S., Clarisse, L., Clerbaux, C., Hurtmans, D., and Coheur, P.-F. Version 2 of the IASI NH<sub>3</sub> neural network retrieval algorithm; near-real time and reanalysed datasets. *Atmos. Meas. Tech.*, 10, 4905–4914, <https://doi.org/10.5194/amt-10-4905-2017> (2017)
- Van Der Molen, J., Beljaars, A. C. M., Chardon, W. J., Jury, W. A., and Faassen, H. G. van. Ammonia volatilization from arable land after application of cattle slurry. 2. Derivation of a transfer model. *Neth. J. Agric. Sci.* <https://doi.org/10.18174/njas.v38i3A.16586> (1990)
- 920 Viatte, C., Abeer, R., Yamanouchi, S., Porter, W., Safieddine, S., Van Damme, M., Clarisse, L., Herrera, B., Grutter, M., Coheur, P.-F., Strong, K., and Clerbaux, C. NH<sub>3</sub> spatio-temporal variability over Paris, Mexico and Toronto and its link to PM<sub>2.5</sub> during pollution events. *EGU Sphere*. <https://doi.org/10.5194/egusphere-2022-413> (2022)
- Viatte, C., Petit, J.-E., Yamanouchi, S., Van Damme, M., Doucerain, C., Germain-Piaulenne, E., Gros, V., Favez, O., Clarisse, L., Coheur, P.-F., Strong, K., and Clerbaux, C. Ammonia and PM<sub>2.5</sub> Air Pollution in Paris during the 2020 COVID Lockdown. *Atmosphere*. <https://doi.org/10.3390/atmos12020160> (2021)
- 925 Viatte, C., Wang, T., Van Damme, M., Dammers, E., Meleux, F., Clarisse, L., Shephard, M. W., Whitburn, S., Coheur, P. F., Cady-Pereira, K. E., and Clerbaux, C. Atmospheric ammonia variability and link with particulate matter formation: A case study over the Paris area. *Atmospheric Chem. Phys.* <https://doi.org/10.5194/acp-20-577-2020> (2020)
- Wentworth, G. R., Murphy, J. G., Gregoire, P. K., Cheyne, C. A. L., Tevlin, A. G., and Hems, R. Soil–atmosphere exchange of ammonia in a non-fertilized grassland: Measured emission potentials and inferred fluxes. *Biogeosciences*. <https://doi.org/10.5194/bg-11-5675-2014> (2014)
- 930 Wesely, M. L. Parameterization of surface resistances to gaseous dry deposition in regional-scale numerical models. *Atmospheric Environ.* 1967. [https://doi.org/10.1016/0004-6981\(89\)90153-4](https://doi.org/10.1016/0004-6981(89)90153-4) (1989)
- Whitburn, S., Damme, M. V., Clarisse, L., Bauduin, S., Heald, C. L., Hadji-Lazaro, J., Hurtmans, D., Zondlo, M. A., Clerbaux, C., and Coheur, P.-F. A flexible and robust neural network IASI-NH<sub>3</sub> retrieval algorithm. *J. Geophys. Res. Atmospheres*. <https://doi.org/10.1002/2016JD024828> (2016)
- 935 Wichink Kruit, R. Surface-atmosphere exchange of ammonia. Ph.D., Wageningen University. Wageningen, Netherlands, <https://edepot.wur.nl/137586> (2010)
- Yang, S., Yuan, B., Peng, Y., Huang, S., Chen, W., Hu, W., Pei, C., Zhou, J., Parrish, D. D., Wang, W., He, X., Cheng, C., Li, X.-B., Yang, X., Song, Y., Wang, H., Qi, J., Wang, B., Wang, C., ... Shao, M. The formation and mitigation of nitrate pollution: Comparison between urban and suburban environments. *Atmospheric Chem. Phys.* <https://doi.org/10.5194/acp-22-4539-2022> (2022)
- 940 Yu, F., Nair, A. A., and Luo, G. Long-Term Trend of Gaseous Ammonia Over the United States: Modeling and Comparison with Observations. *J. Geophys. Res. Atmospheres*. <https://doi.org/10.1029/2018JD028412> (2018)

- 945 Zhang, L., Wright, L. P., and Asman, W. a. H. Bi-directional air-surface exchange of atmospheric ammonia: A review of measurements and a development of a big-leaf model for applications in regional-scale air-quality models. *J. Geophys. Res. Atmospheres*. <https://doi.org/10.1029/2009JD013589> (2010)

**Mis en forme :** Bibliographie, Justifié, Taquets de tabulation :  
Pas à 3,84 cm